SEMARAK ILMU PUBLISHING

Journal of Advanced Research in Fluid Mechanics and Thermal Sciences

Journal homepage:
https://semarakilmu.com.my/journals/index.php/fluid_mechanics_thermal_sciences/index
ISSN: 2289-7879

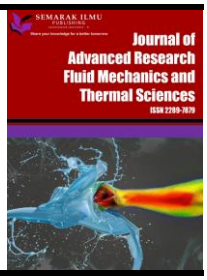

Improve Solutions of Differential Transform Method for Jeffrey Hamel Magneto-hydrodynamic Non-Newtonian Casson Fluid Flow Problem

Ahmed Rasheed Khlefha[1,*], Abeer Majeed Jasim[2]

[1] Department of Mathematics, College of Education, University of Sumer, Thi-Qar, Iraq
[2] Department of Mathematics, College of Science, University of Basrah, Basrah, Iraq

ARTICLE INFO

Article history:
Received 20 October 2023
Received in revised form 19 January 2024
Accepted 1 February 2024
Available online 29 February 2024

Keywords:
Differential transform method; optimal differential transform method; Jeffery Hamel Flow; Casson fluid

ABSTRACT

In this article, Magneto-hydrodynamic flow of a non-Newtonian Casson fluid in converging and diverging channels subject to stretching -shrinking cases is an important problem in the field of fluid flow that has been highlighted by the combination of the differential transformation method and the optimal method so-called optimal differential transformation method (ODTM). In this synthesis that is used achieves improved analytical results for this problem. This study examines the impact of several developing characteristics, including channel angle, stretching-shrinking parameter, Casson fluid parameter, Hartmann number, and Reynolds number with the velocity profiles. Results obtained from the DTM and the numerical method BVP4c are compared to those resulting from ODTM which consist of the collocation differential transform method (CDTM), the sub-domain differential transform method (SDTM), the least squares differential transform method (LSDTM), and the Galerkin differential transform method (GDTM). The comparison shows that the percentage errors of the optimal methods (ODTM) are more accurate than those of the DTM for a similar number of parts of the repeated series over a wide range of physical parameters. Finally, it can be said that the results of the proposed method for third-order nonlinear Jeffrey Hamel flow in the non-Newtonian Casson fluid problem are high accuracy.

1. Introduction

The model of non-Newtonian Jeffery Hamel flow of Casson fluid is the topic under consideration and is generally recognized as a valuable subject for investigating many aspects of industrial applications, including but not limited to automotive, mechanical, chemical, agricultural, and civil engineering processes. Significant progress has been achieved in the use of Jeffrey Hamel's problems, particularly in the domains of fluid dynamics, chemical engineering, and aeronautical engineering. Various applications of this technology include chemically vaporized deposition reactors, laser turbines using high-current arcs, industrial equipment for area growth or reduction, as well as gas condensers and pipe components. The examination of thermal radiation in the context of the well-

* *Corresponding author.*
E-mail address: arkdsh85@gmail.com

https://doi.org/10.37934/arfmts.114.2.80105

known Jeffery Hamel flow issue presents a significant academic and technological difficulty for the field of aviation. This problem involves the study of converging-diverging streams that experience either contraction or expansion, leading to notable implications. The Jeffery-Hamel flow pertains to the behavior of a confined fluid that is two-dimensional, viscous, and incompressible. This flow occurs between two planes that are positioned at a certain angle, either divergent or convergent. Magneto-hydrodynamics (MHD) is an academic discipline that investigates the dynamics and characteristics of electrically conductive fluids about their magnetic properties. Some examples of magnetic fluids contain several substances, including liquid metals, plasmas, and salts. The word magneto-hydrodynamics is composed of "magneto," which refers to a magnetic field; "hydro," which pertains to water; and "dynamics," which relates to movement [1]. The significance of investigating the problems surrounding Jeffery Hamel is in the ability to control fluid flow via the manipulation of static electrical field strength. The dynamics of fluid motion in the presence of a magnetic field exhibit notable disparities compared to those in its absence. The analysis of Jeffery Hamel's concerns with the static electrical field on the conductive fluid is conducted using magnetic amplitude as a control parameter [2-4]. Several researchers have conducted studies on the behavior of Casson fluid using various experiments. One potential research focus is investigating the impact of Soret and Dufour's effects on the magneto-hydrodynamic flow of Casson fluid by the use of semi-analytical techniques, as shown in previous studies by several researchers, Jalili *et al.,* [5] investigated the fluid dynamics in porous materials of different forms utilizing magnetohydrodynamic/hydrodynamic and heat transfer techniques. Jasim and Al-Saif [6] used several analytical methods to solve the equations governing fluid flow problems Jalili *et al.,* [7] created the HAN technique to estimate an analytical solution for the flow of non-Newtonian Casson fluid in a porous medium. Sarada *et al.,* [8] presented a comprehensive analysis of multiple research that examined the factors influencing the characteristics of nanofluids, which are known to enhance thermal conductivity. This analysis encompassed various features and scenarios. Jalili *et al.,* [9] all heat transmission processes in non-Newtonian fluid flow have been thoroughly examined. AGM and FEM approaches have been employed to solve this fluid flow's governing equations, exhibiting perfect agreement. In their study, Alhadhrami *et al.,* [10] investigated the numerical simulation of the impact of local thermal non-equilibrium on the flow and heat transmission of a non-Newtonian Casson fluid in a porous media. The study conducted by Li *et al.,* [11] nanotechnology has made significant progress, particularly in the development of nanofluids. These are hybrid fluids that contain small metallic particles, enhancing their thermophysical properties. This field is currently a major focus in applied mathematics's industrial and technical applications. In their study, Gowda *et al.,* [12] employed a hybrid method that combined the RKF-45 technique with a shooting approach to investigate the behaviour of an incompressible and conducting electrically Casson-Maxwell fluid confined between two uniformly stretchable discs. Jalili *et al.,* [13] was intrigued by the occurrence of entropy formation in rectangular containers filled with nanofluids. Gowda *et al.,* [14] studied the interlayer of nanofluids using Jeffrey nanofluid. Kumar *et al.,* [15] examined the impact of thermophoresis and Brownian motion on the flow of nanofluids over a curved extension plate (CSS). The study incorporated the Cattaneo-Christoph thermal flow and Stefan blow (SB) conditions to analyze the properties of heat and mass transportation. Kumar *et al.,* [16] investigated convective heat transfer and KK bonding, to model the flow of nanofluids on a curved extended plate. Recently, Zhao's *et al.,* [17] multiple researches have investigated the movement of various substances across a range of surfaces. Abdulridah and Jasim [18] studied the flow and heat transfer of a nanofluid through a converging or diverging channel in a porous medium for the flow problem of Jasim [19] and Khan *et al.,* [20] examined the fluid flow in different types of flow channels. Kumar *et al.,* [21] examined the movement of electrically conductive fluids that have both convective and hydromagnetic properties in a vertical loop. They applied principles from

thermodynamics to analyse the system, taking into account the influence of an induced magnetic field, entropy generation, and time-periodic boundary conditions. Jalili *et al.,* [22] examined the dispersion of temporary temperature in a mobile plate with a thermal conductivity that is highly influenced by heat and the heat transfer coefficient. The majority of problems related to fluid mechanics are fundamentally expressed in a nonlinear form and are often associated with nonlinear ordinary and partial differential equations, respectively. The current analytical techniques have been inadequate for appropriately assessing non-linear equations of this kind. To address this kind of problem, it is necessary to use numerical or semi-analytical methods. The researchers express a preference for using specific accepted methods for solving problems in many fields including decomposing approach, perturbation approach, iteration approach, homotopy analysis, optimum asymptotic approaches, and differential transform approach. Semi-analytical and numerical approaches are often used because of their enhanced accuracy and efficiency in generating findings. The present paper utilizes the differential transform method [23]. This approach is a robust and semi-exact strategy that does not rely on the presence of either big or tiny components. This approach offers significant advantages compared to previous approximated semi-exact methods. The resolution of diverse types of equations that are differential was advantageous, including difference equations, eigenvalues issues, nonlinear integrals, high index differential-algebraic mathematical equations, fractional formulas, pantograph formulas, nonlinear oscillations, and integrodifferential equations without imposing constrictive suppositions This encompasses techniques such as the linearization process, discretization, and the mitigation of round-off errors. Numerous academics have used the differential transform method to address a wide range of fluid field issues. In their study, Hatami *et al.,* [24] used the differential transform method to deal with the issue of the non-Newtonian flow of fluid in a plate shape. In a recent study, Sobamowo [25] used the DTM to analyse a two-dimensional fluid issue occurring inside a porous channel. Sowmya *et al.,* [26,27] investigated the thermal characteristics of a longitudinal fin and moving rod in the presence of internal production of heat, considering the effects of natural radiation and convection. Kumar *et al.,* [28] predicted the thermal variation in the fin of rectangular configuration with convection-radiation impact and delineated the nature of thermal dispersion for different fin materials by using DTM. One of the primary benefits of the differential transform method is its ability to effectively solve nonlinear problems in mathematics without needing linearization other the discretization. Therefore, the approach does not claim to be free from mistakes associated with the process of discretization Additionally, it reduces the computational complexity and applies to a wide range of problems in mathematics with simplicity. The implementation of the DTM has shown effective application in multiple fields such as dynamics of fluids, multi-physical mechanics, and heat transfer systems throughout the present century, study on the fluid flow problem in a plane Couette configuration, analysis of vibration in a state of unrestricted motion, the topic of discussion is the flow of micropolar fluids, an examination of the flow of non-Newtonian nanofluids, the text discusses acoustic and wave propagation concerns and the use of a viscoelastic Winkler foundation, modelling the process of intestinal transit, convection driven by temperature and solute gradients in porous medium [29-34]. There exist several straightforward and precise approximation methods for the solution of differential equations called the weighted residual methods. Collocation, least square, and Galerkin methods are instances of the weighted residual methods. Stern and Rasmussen [35] employed the collocation method as a means to solve a third-order linear differential equation. Nabati *et al.,* [36] proposed the collocation method to address the equation of thermal performance within a porous medium. The possibility of utilizing the orthogonal collocation method for solving the diffusivity equation in a radial transient flow system was investigated by Vaferi *et al.,* [37]. Biswal *et al.,* [38] used the least-squares method to resolve the equations which govern that describe the flow of

nanofluid in a semi-porous channel. In their study, Shaoqin and Huoyuan [39] conducted the development and analysis of least-squares approximations for the incompressible magneto-hydrodynamic equations. Abbaszadeh *et al.,* [40] introduced the Galerkin method for solving the Navier-Stokes equation coupled with the heat transfer equation. Hendi and Albugami [41] employed collocation and Galerkin methods to address the solution of Fredholm-Volterra integral equations. Liberty and Miracle [42] used weighted residual methods to solve boundary value problems. After that, a second-order differential equation was solved using all methods to evaluate its efficiency and stability. Zhou *et al.,* [43] applied a subdomain method to replicate the kernel approximation technique. Subsequently, the subdomains were created using non-overlapping Voronoi cells in order to establish a localized model with limited strength within these subdomains. In the present article, we will provide a novel approximation method referred to as the optimal differential transform method which consists of the collocation differential transform method, the sub-domain differential transform method, the least squares differential transform method, and the Galerkin differential transform method as in Figure 1. The primary characteristic of the optimal differential transform method is its ability to achieve rapid convergence while minimizing computing expenses. To validate the findings obtained from the optimal differential transform method, the same problems were also addressed using the differential transform method and the numerical technique BVP4c. The remainder of the parts are structured in the following, the governing problem in section second, the ideal basis of the differential transform method for ordinary differential equations in section three, the application of the differential transform method and BVP4c in section four, improving the analytical aspect in section five, the convergence test in section six, discuss Tabular given in section seven, discuss graphics given in section eight. Finally, the conclusion is presented in section nine.

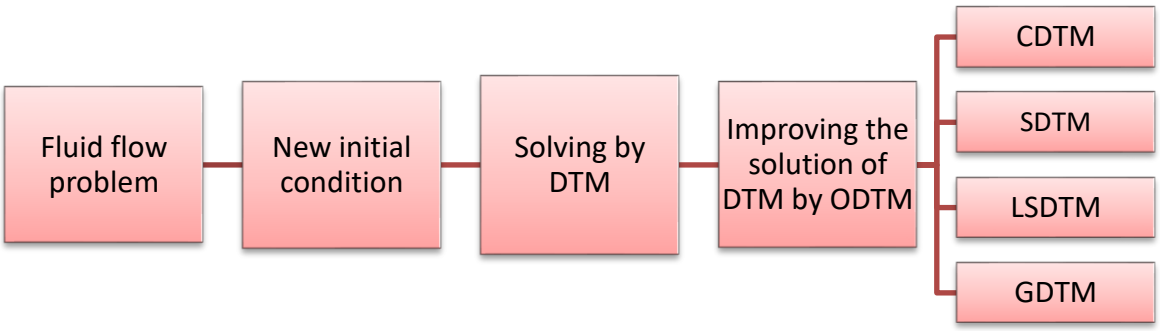

Fig. 1. Executive plan for basic work steps

2. The Governing of the Problem

The present study focuses on the analysis of the two-dimensional incompressible magneto-hydrodynamic flow of a non-Newtonian Casson fluid between two expanding or shrinking barriers, as described by Gowda *et al.,* [12] in Figure 2 depicts the structural characteristics of the magneto-hydrodynamic (MHD) Jeffery Hamel flow. The space between both walls is denoted as 2ε. We may analyze two situations in the following manner:

(a) Converging wall when $\varepsilon < 0$.
(b) Diverging wall when $\varepsilon > 0$.

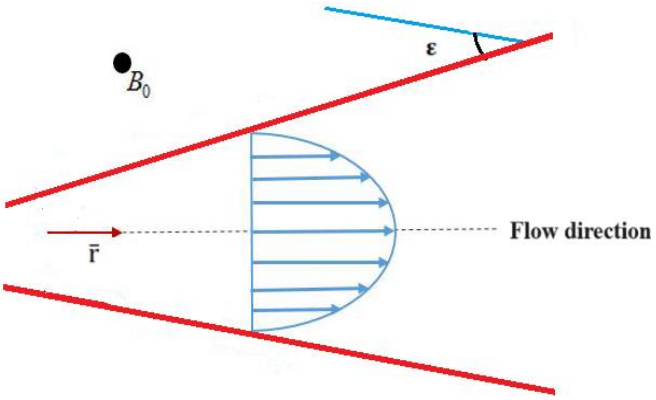

Fig. 2. The Geometry of the Jeffery Hamel Flow

The fundamental model that characterizes an incompressible non-Newtonian Casson fluid is outlined in the following manner.

$$\tau_{ij} = \begin{cases} 2\left(\mu_B + \frac{\mathcal{P}_y}{\sqrt{2\,\dot{\pi}}}\right)\dot{C}_{ij}\,, \dot{\pi} < \dot{\pi}_c \\ 2\left(\mu_B + \frac{\mathcal{P}_y}{\sqrt{2\,\dot{\pi}}}\right)\dot{C}_{ij}\,, \dot{\pi} > \dot{\pi}_c \end{cases}, \tag{1}$$

where μ_B is the non-Newtonian fluid's elastic fluid velocity, $\mathcal{P}_y$ is the pressure of the fluid, $\dot{\pi}$ is the product of the component of deformation rate with itself which mean $\dot{\pi} = \dot{C}_{ij}\dot{C}_{ij}$ with $\dot{C}_{ij}$ is(i,j) component of the deformation rate, and $\dot{\pi}_c$ is a critical value of this product dependent mostly on the non-Newtonian model. For this problem, the conservation laws of mass and momentum are:

$$\nabla \cdot \bar{U} = 0\,, \tag{2}$$

$$\bar{\rho}\left(\frac{\partial \bar{U}}{\partial t} + (\nabla \cdot \bar{U})\bar{U}\right) = -\nabla \bar{p} + \nabla \cdot \bar{\tau}_{ij} + \bar{g}_B. \tag{3}$$

By cylinder coordinates are used to transform the continuity and momentum equations from Eq. (1) to Eq. (3) for this problem,

$$\frac{1}{\bar{r}}\frac{\partial(\bar{r}\bar{u}_{\bar{r}}(\bar{r},\bar{\varphi}))}{\partial \bar{r}} = 0, \tag{4}$$

$$-\bar{u}_{\bar{r}}(\bar{r},\bar{\theta})\frac{\partial \bar{u}_{\bar{r}}(\bar{r},\bar{\theta})}{\partial \bar{r}} - \frac{1}{\bar{\rho}}\frac{\partial \dot{p}}{\partial \bar{r}} + \psi\left(1+\frac{1}{\gamma}\right)\left(\frac{\partial^2 \bar{u}_{\bar{r}}(\bar{r},\bar{\theta})}{\partial \bar{r}^2} + \frac{1}{\bar{r}}\frac{\partial \bar{u}_{\bar{r}}(\bar{r},\bar{\theta})}{\partial \bar{r}} + \frac{1}{\bar{r}^2}\frac{\partial^2 \bar{u}_{\bar{r}}(\bar{r},\bar{\theta})}{\partial \bar{\theta}^2} - \frac{\bar{u}_{\bar{r}}(\bar{r},\bar{\theta})}{\bar{r}^2}\right) - \frac{\ell \Sigma_0}{\sigma \bar{r}^2}\bar{u}_{\bar{r}} = 0, \tag{5}$$

$$-\frac{1}{\bar{\rho}\bar{r}}\frac{\partial \dot{p}}{\partial \bar{\theta}} + \frac{2\psi}{\bar{r}^2}\left(1+\frac{1}{\gamma}\right)\left(\frac{\partial \bar{u}_{\bar{r}}(\bar{r},\bar{\theta})}{\partial \bar{\theta}}\right) = 0, \tag{6}$$

where $\dot{p}$ is the pressure, $\bar{u}_{\bar{r}}$ is the velocity in radial direction, $\bar{\rho}$ is the fluid density, $\gamma = \frac{\dot{\mu_B}\sqrt{2\pi}}{P_y}$ is the fluid parameter, ψ is kinematic viscosity and ℓ is the conductivity of the fluid and denote $\dot{\Sigma}_\circ$ to the electromagnetic induction.

$$\bar{u}_{\bar{r}} = \bar{u}_w = \frac{\bar{s}}{\bar{r}}\,, \bar{\theta} = \pm\varepsilon,$$

$$\bar{u}_{\bar{r}} = \frac{\bar{u}_{c\bar{r}}}{\bar{r}} \, , \frac{\partial \bar{u}_{\bar{r}}(\bar{r},\bar{\theta})}{\partial \bar{\theta}} = 0 \text{ at } \bar{\theta} = 0. \tag{7}$$

where $\bar{u}_{c\bar{r}}$ denotes the movement along the center line, $\bar{u}_w$ the velocity along the channel walls, and $\bar{s}$ the rate of stretching and contracting. Eq. (4) is integrated with regard to $\bar{r}$, following is the continuation a formula:

$$\mathcal{Y}(\bar{\theta}) = \bar{r}\, \bar{u}_{\bar{r}}(\bar{r},\bar{\theta}) \, , \tag{8}$$

The use of dimensionless variables, as described by Eq. (8), enables the issue to be expressed in a dimensionless form.

$$Y(\xi) = \frac{\mathcal{Y}(\bar{\theta})}{\bar{\mathcal{Y}}_{c\bar{r}}} \, , \xi = \frac{\bar{\theta}}{\varepsilon} \, , \bar{r} = \frac{\bar{u}_{c\bar{r}}}{\bar{r}} Y(\xi). \tag{9}$$

From Eq. (9), we get the essential derivatives,

$$\frac{\partial \bar{u}_{\bar{r}}}{\partial \bar{\varphi}} = \frac{\bar{u}_{c\bar{r}}}{\varepsilon \bar{r}} \frac{dY(\xi)}{d\xi} \, , \frac{\partial^3 \bar{u}_{\bar{r}}}{\partial \bar{\varphi}^3} = \frac{\bar{u}_{c\bar{r}}}{\varepsilon^3 \bar{r}} \frac{d^3 Y(\xi)}{d\xi^3} \, , \frac{\partial^3 \bar{u}_{\bar{r}}}{\partial \bar{r}^2 \, \partial \bar{\theta}} = \frac{2\bar{u}_{c\bar{r}}}{\varepsilon \bar{r}^3} \frac{dY(\xi)}{d\xi} \, , \tag{10}$$

$$\frac{\partial \bar{u}_{\bar{r}}}{\partial \bar{r}} = -\frac{\bar{u}_{c\bar{r}}}{\bar{r}^2} Y(\xi) \, , \frac{\partial^2 \bar{u}_{\bar{r}}}{\partial \bar{\theta} \, \partial \bar{r}} = -\frac{\bar{u}_{c\bar{r}}}{\varepsilon \bar{r}^2} \frac{dY(\xi)}{d\xi} \, , \frac{\partial^2 \bar{u}_{\bar{r}}}{\partial \bar{r}^2} = \frac{2\bar{u}_{c\bar{r}}}{\varepsilon \bar{r}^3} \frac{dY(\xi)}{d\xi} \, ,$$

Integrating Eq. (6) with respect to $\bar{\theta}$ then by derivation the resulted equation with respect to $\bar{r}$, the continuity rule is:

$$\frac{1}{\bar{\rho}} \frac{\partial \dot{p}}{\partial \bar{r}} = \left(1 + \frac{1}{\gamma}\right) \left(-\frac{2\psi}{\bar{r}^2} \bar{u}_{\bar{r}}(\bar{r},\bar{\theta}) + \frac{2\psi}{\bar{r}} \frac{\partial \bar{u}_{\bar{r}}(\bar{r},\bar{\theta})}{\partial \bar{\theta}} \right), \tag{11}$$

Now, putting Eq. (10) into Eq. (11) give up,

$$\frac{1}{\bar{\rho}} \frac{\partial \dot{p}}{\partial \bar{r}} = \left(1 + \frac{1}{\gamma}\right) \left(\frac{-4\psi}{\bar{r}^3} \bar{u}_{c\bar{r}} Y(\xi) \right), \tag{12}$$

Substituting Eq. (10) and Eq. (12) into Eq. (5) we get,

$$\frac{\bar{u}_{\bar{r}c}^2}{\bar{r}^3} Y^2(\xi) + \left(1 + \frac{1}{\gamma}\right) \left(\frac{4\psi}{\bar{r}^3} \bar{u}_{\bar{r}} Y(\xi) \right) + \psi \left(1 + \frac{1}{\gamma}\right) \left(2 \frac{\bar{u}_{\bar{r}c}}{\bar{r}^3} Y(\xi) - \frac{1}{\bar{r}} \frac{\bar{u}_{\bar{r}c}}{\bar{r}^2} Y(\xi) + \frac{1}{\bar{r}^3} \frac{\bar{u}_{\bar{r}c}^2}{\varepsilon^2} \frac{d^2 Y(\xi)}{d\xi^2} - \frac{\bar{u}_{\bar{r}}}{\bar{r}^3} Y(\xi) \right) -$$
$$\frac{\ell {\Sigma_0}^2}{\bar{\rho} \bar{r}^2} \frac{\bar{u}_{\bar{r}c}}{\bar{r}} Y(\xi) = 0. \tag{13}$$

After simplistic analysis from the above rule, the ultimate section is taken as,

$$\bar{u}_{\bar{r}c} \, Y^2(\xi) + 4\psi \left(1 + \frac{1}{\gamma}\right) Y(\xi) + \psi \left(1 + \frac{1}{\gamma}\right) \frac{1}{\varepsilon^2} \frac{d^2 Y(\xi)}{d\xi^2} - \frac{\ell {\Sigma_0}^2}{\bar{\rho}} Y(\xi) = 0, \tag{14}$$

Differentiate the Eq. (14) with respect to ξ,

$$\bar{u}_{\bar{r}c} Y(\xi) \frac{dY(\xi)}{d\xi} + 4\psi \left(1 + \frac{1}{\gamma}\right) \frac{dY(\xi)}{d\xi} + \psi \left(1 + \frac{1}{\gamma}\right) \frac{1}{\varepsilon^2} \frac{d^3 Y(\xi)}{d\xi^3} - \frac{\ell {\Sigma_0}^2}{\bar{\rho}} \frac{dY(\xi)}{d\xi} = 0, \tag{15}$$

Multiply both sides of Eq. (15) by $\frac{\varepsilon}{\psi}$ we have:

$$\left(1+\frac{1}{\gamma}\right)\frac{d^3\mathcal{Y}(\xi)}{d\xi^3}+2\varepsilon R_e\mathcal{Y}(\xi)\frac{d\mathcal{Y}(\xi)}{d\xi}+\varepsilon^2\left(4\left(1+\frac{1}{\gamma}\right)-H_a\right)\frac{d\mathcal{Y}(\xi)}{d\xi}=0, \tag{16}$$

With boundary conditions

$$\mathcal{Y}(0)=1,\frac{d\mathcal{Y}(0)}{d\xi}=0\,,\mathcal{Y}(1)=\bar{\chi}. \tag{17}$$

Between the two planes classify, $R_e=\frac{\varepsilon\bar{\mathrm{U}}_{\bar{\mathrm{r}}\mathrm{c}}}{\psi}$ is Reynolds number and $H_a=\frac{\delta{\Sigma_0}^2}{\bar{\rho}\psi}$ is Hartmann number, we can classify to two cases as,

(a) Convergent channel: $\varepsilon<0\,,\bar{\mathrm{u}}_{\bar{\mathrm{r}}\mathrm{c}}<0\,,$
(b) Divergent channel: $\varepsilon>0\,,\bar{\mathrm{u}}_{\bar{\mathrm{r}}\mathrm{c}}>0\,.$

The definition of a $\bar{\chi}$ is stretching-shrinking parameter. Physically, there are three cases can be summated as follows:

(a) Shrinking channel $\bar{\chi}<0,$
(b) Fix surface $\bar{\chi}=0,$
(c) Stretching channel $\bar{\chi}>0.$

Finally, the values of the friction coefficient of a skin can be obtained,

$$\bar{\chi}_y=\left.\frac{\bar{\mathrm{r}}^2\tau_{\bar{\mathrm{r}}\bar{\theta}}}{\bar{\mathrm{u}}_{\bar{\mathrm{r}}\mathrm{c}}^2}\right|_{\xi=1}=\frac{1}{\dot{R_e}}\left(1+\frac{1}{\gamma}\right)\frac{d\mathcal{Y}(1)}{d\xi}\,. \tag{18}$$

3. The Ideal Basic Differential Transform Method for Ordinary Differential Equations

The differential transformation technique was developed by Zhou in 1986. This approach was developed to solve non-linear initial value problems. To construct idea the differential transformation technique, we can be defined the ordinary differential equation as follows:

$$\mathcal{L}[\mathcal{Y}(\xi)]+\mathbb{N}[\mathcal{Y}(\xi)]-\mathcal{F}(\xi)=0, \tag{19}$$

where ξ denotes an independent variable, $\mathcal{Y}(\xi)$ is unknown function and $\mathcal{F}(\xi)$ is known function. $\mathcal{L}$ and $\mathbb{N}$ are boundary linear and nonlinear operators. The following basic definitions and optimal differential transformation procedures are introduced for the function (ξ):

$$\mathcal{W}(k)=\frac{1}{\bar{k}!}\left(\frac{d^{\bar{k}}\mathcal{Y}(\xi)}{d\xi^{\bar{k}}}\right)_{\xi=\xi_0}. \tag{20}$$

Now, can be noticed $\mathcal{Y}(\xi)$ is the original function which stated in practical applications as infinite series and $\mathcal{W}(k)$ is the transformed function. The inverse transform of the function $\mathcal{W}(k)$ can be expressed as follows:

$$\mathcal{Y}(\xi)=\sum_{k=0}^{\infty}\mathcal{W}(k)(\xi-\xi_0)^{\bar{k}}. \tag{21}$$

Substituting Eq. (20) and Eq. (21) into Eq. (19), yield

$$\mathcal{L}[\sum_{\bar{k}=0}^{\infty}\frac{(\xi-\xi_0)^{\bar{k}}}{\bar{k}!}\left(\frac{d^{\bar{k}}y(\xi)}{d\xi^{\bar{k}}}\right)_{\xi=\xi_0}]+\mathbb{N}[\sum_{\bar{k}=0}^{\infty}\frac{(\xi-\xi_0)^{\bar{k}}}{\bar{k}!}\left(\frac{d^{\bar{k}}y(\xi)}{d\xi^{\bar{k}}}\right)_{\xi=\xi_0}]-\mathcal{F}(\xi)=0. \quad (22)$$

Consequently, can be reassigned the optimal coefficients Π_k, $k=0,1,2,\dots,n$ in obtained series solution in Eq. (22) to get the residual function:

$$\mathcal{R}(\xi,\Pi_0,\ \Pi_1,\ \Pi_2,\dots,\Pi_n)=\mathcal{L}[\mathcal{Y}(\xi;\Pi_0,\Pi_1,\Pi_2,\dots,\Pi_n)]+\mathbb{N}[\mathcal{Y}(\xi;\Pi_0,\Pi_1,\Pi_2,\dots,\Pi_n)]-\mathcal{F}(\xi),$$

An approximate analytical solution can be defined by the presence of optimal coefficients as follows:

$$\mathcal{Y}(\xi;\Pi_0,\Pi_1,\Pi_2,\dots,\Pi_n)=\sum_{\bar{k}=0}^{\infty}\Pi_k\frac{(\xi-\xi_0)^{\bar{k}}}{\bar{k}!}\left(\frac{d^{\bar{k}}y(\xi)}{d\xi^{\bar{k}}}\right)_{\xi=\xi_0}. \quad (23)$$

The fundamental, often employed differential transform mathematical operations are derived and are given in Table 1, as follows:

Table 1
The functions of differential Transformation

Original function	Transformed function
$\boldsymbol{\mathcal{Y}(\xi)=t(\xi)\pm v(\xi)}$	$\mathcal{W}(k)=T(k)\pm V(k)$
$\boldsymbol{\mathcal{Y}(\xi)=\epsilon t(\xi)}$	$\mathcal{W}(k)=\epsilon T(k)$, ϵ is constant
$\boldsymbol{\mathcal{Y}(\xi)=t(\xi)v(\xi)}$	$\mathcal{W}(k)=\sum_{i=0}^{\bar{k}}T(i)V(k-i)$
$\boldsymbol{\mathcal{Y}(\xi)=\frac{d^n t(\xi)}{d\xi^n}}$	$\mathcal{W}(k)=\frac{(k+n)!}{k!}T(k+n)$

4. The Application of Differential Transform Method and BVP4c

In this section, we use both the differential transform approach and BVP4c to address the problem of magneto-hydrodynamic Casson fluid Jeffery Hamel flow. The solutions provided may be classified as approximate analytical and numerical methods, and can be summarized as follows:

(i) Analytical Aspect

The iterative method for Eq. (16) is developed utilizing Table 1 of the differential transform method in the following manner:

$$\left(1-\frac{1}{\gamma}\right)\left(\bar{k}+1\right)\left(\bar{k}+2\right)\left(\bar{k}+3\right)\mathcal{W}\left(\bar{k}+3\right)-2\boldsymbol{\varepsilon}R_e\sum_{\mathrm{i}=0}^{\mathrm{k}}(\mathrm{i}+1)\mathcal{W}(\mathrm{i}+1)\mathcal{W}(\mathrm{k}-\mathrm{i})-$$
$$\varepsilon^2\left(4\left(1+\frac{1}{\gamma}\right)-H_a\right)(\mathrm{k}+1)\mathcal{W}(\mathrm{k}+1)=0, \quad (24)$$

The boundary conditions can be written as follows:

$$\mathcal{W}(0)=1\,,\mathcal{W}(1)=0\,,\mathcal{W}(2)=\Pi, \quad (25)$$

where Π can be determined using $\mathcal{Y}(1) = \bar{\chi}$ and using the iterative of Eq. (16) and Eq. (17) and we get approximant analytical solutions for $\mathcal{Y}$.

$$\mathcal{Y}_0(\xi) = 1,$$

$$\mathcal{Y}_2(\xi) = 1 + \Pi\xi^2,$$

$$\mathcal{Y}_4(\xi) = 1 + \Pi\xi^2 + \left(\frac{\Pi\varepsilon\left((\gamma(\mathrm{H}-4)-4)\varepsilon-2\gamma R_e\right)}{12(\gamma+1)}\right)\xi^4,$$

$$\mathcal{Y}_6(\xi) = 1 + \Pi\xi^2 + \left(\frac{\Pi\varepsilon\left((\gamma(\mathrm{H}-4)-4)\varepsilon-2\gamma R_e\right)}{12(\gamma+1)}\right)\xi^4 + \frac{\Pi\varepsilon}{360(\gamma+1)}\left(((\mathrm{H}-4)^2\varepsilon^3 - 4R_e (\mathrm{H}-4)\varepsilon^2 + 4\varepsilon R_e^2 - 12\Pi R_e)\gamma^2 + ((32-8\mathrm{H})\varepsilon^3 + 16\varepsilon^2 R_e - 12\Pi R_e)\gamma + 1616\varepsilon^3\right)\xi^6,$$

$$\mathcal{Y}_8(\xi) = 1 + \Pi\xi^2 + \left(\frac{\Pi\varepsilon\left((\gamma(\mathrm{H}-4)-4)\varepsilon-2\gamma R_e\right)}{12(\gamma+1)}\right)\xi^4 + \frac{\Pi\varepsilon}{360(\gamma+1)}\left(((\mathrm{H}-4)^2\varepsilon^3 - 4R_e (\mathrm{H}-4)\varepsilon^2 + 4\varepsilon R_e^2 - 12\Pi R_e)\gamma^2 + ((32-8\mathrm{H})\varepsilon^3 + 16\varepsilon^2 R_e - 12\Pi R_e)\gamma + 1616\varepsilon^3\right)\xi^6 + \frac{1}{20160(\gamma+1)}\Big(\left(\varepsilon^2\left((\mathrm{H}-4)\varepsilon - 2R_e\right)\gamma - 4\varepsilon\right)\left(\varepsilon^2\left((\mathrm{H}-4)\varepsilon - 2R_e\right)\gamma - 4\varepsilon\right)\left(\gamma^2\left((\mathrm{H}-4)^2\varepsilon^3 - 4R_e(\mathrm{H}-4)\varepsilon^2 + 4\varepsilon R_e^2 - 72\Pi R_e\right)\right) + \left((32-8\mathrm{H})\varepsilon^3 + 16\varepsilon^2 R_e - 72\Pi R_e\right) + 16\varepsilon^3\Big)\Big)\xi^8,$$

$$\vdots$$

The required approximate analytical solution of $\mathcal{Y}(\xi)$ is,

$$\mathcal{Y}(\xi) = 1 + \Pi\xi^2 + \left(\frac{\Pi\varepsilon\left((\gamma(\mathrm{H}-4)-4)\varepsilon-2\gamma R_e\right)}{12(\gamma+1)}\right)\xi^4 + \frac{\Pi\varepsilon}{360(\gamma+1)}\left(((\mathrm{H}-4)^2\varepsilon^3 - 4R_e (\mathrm{H}-4)\varepsilon^2 + 4\varepsilon R_e^2 - 12\Pi R_e)\gamma^2 + ((32-8\mathrm{H})\varepsilon^3 + 16\varepsilon^2 R_e - 12\Pi R_e)\gamma + 1616\varepsilon^3\right)\xi^6 + \frac{1}{20160(\gamma+1)}\Big(\left(\varepsilon^2\left((\mathrm{H}-4)\varepsilon - 2R_e\right)\gamma - 4\varepsilon\right)\left(\varepsilon^2\left((\mathrm{H}-4)\varepsilon - 2R_e\right)\gamma - 4\varepsilon\right)\left(\gamma^2\left((\mathrm{H}-4)^2\varepsilon^3 - 4R_e(\mathrm{H}-4)\varepsilon^2 + 4\varepsilon R_e^2 - 72\Pi R_e\right)\right) + \left((32-8\mathrm{H})\varepsilon^3 + 16\varepsilon^2 R_e - 72\Pi R_e\right) + 16\varepsilon^3\Big)\Big)\xi^8 + \cdots. \quad (26)$$

(ii) Numerical Aspect

The bvp4c solver in MATLAB is employed for the solution of Eq. (16), which represents a nonlinear ordinary differential equation under the presence of initial and boundary conditions as described in Eq. (17). The proposed solution entails the utilization of the finite difference code with the accuracy of fourth order. In order to apply the solution, it is necessary to rephrase the equation as a collection of equivalent first-order ordinary differential equations, which afterward transform into

$$\mathcal{Y}(\xi) = \mathcal{F}_1, \frac{d\mathcal{Y}(\xi)}{d\xi} = \mathcal{F}_2, \frac{d^2\mathcal{Y}(\xi)}{d\xi^2} = \mathcal{F}_3,$$
$$\frac{d\mathcal{F}_3}{d\xi} = \frac{-\varepsilon\mathcal{F}_2}{(1+\gamma)}\left(-2\gamma R_e\mathcal{F}_1 - 4\varepsilon + \varepsilon\gamma(H_a - 4)\right). \quad (27)$$

From the boundary conditions (17), we obtain that

$$\mathcal{F}_1(0) = 1\,, \mathcal{F}_2(0) = 0\,, \mathcal{F}_2(1) = \mathcal{T}. \tag{28}$$

Eq. (37) and Eq. (38) had been numerically integrated to an established endpoint in order to find an initial value problem. The need to use the MATLAB package necessitated all of these simplifications. Then, by executing this program with a 0.1 step size, the range from 0 to 1 and back is determined.

5. Improve Analytical Aspect

To improve the approximate analytical solution obtained from DTM in Eq. (26) which includes $\xi^2, \xi^4, \xi^6, \xi^8, \xi^{10}$ assume the approximate analytical solution in the following form:

$$\tilde{\mathcal{Y}}(\xi) = \Pi_0 + \Pi_1\xi^2 + \Pi_2\xi^4 + \Pi_3\xi^6 + \Pi_4\xi^8 + \Pi_5\xi^{10}. \tag{29}$$

To determine the appropriate values for $\Pi_k, k = 0,1,2,4,5$ we employ the weighted residual methods to get the best coefficients for ξ. There was a computational method known as the Weighted Residuals method that was utilized for approximating solutions to differential equations. Let us consider the application of a differential operator $\mathcal{D}$ on a given function $\mathcal{Y}$, resulting in the generation of a new function $\tilde{f}$,

$$\mathcal{D}\big(\mathcal{Y}(\xi)\big) = \tilde{f}(\xi)\,. \tag{30}$$

The approximation of the variable $\mathcal{Y}$ is commonly achieved by expressing it as a linear combination of basic functions $\tilde{\mathcal{Y}}$ selected from a set that is linearly independent. This can be interpreted as,

$$\mathcal{Y} \cong \tilde{\mathcal{Y}} = \textstyle\sum_{i=1}^{n} \Pi_i\, \widetilde{\emptyset}_i\,. \tag{31}$$

When the differential operator $\mathcal{D}$ is applied, the outcome of the operations typically does not yield $\tilde{f}(\xi)$. Therefore, it is expected that an error or residual will be present

$$R(\xi) = \mathcal{D}\left(\tilde{\mathcal{Y}}(\xi)\right) - \tilde{f}(\xi) \neq 0. \tag{32}$$

The concept within the context of Weighted Residual Methods involves the objective of achieving a zero residual in an averaged manner across the entire domain. In other words:

$$\textstyle\int_a^b \mathcal{R}(\xi)\, \widetilde{w}_i d\xi, i = 1,2,\dots,n\,. \tag{33}$$

The total number of weight functions, denoted as $\widetilde{w}_i$ is precisely equivalent to the number of unknown constants, represented as $\Pi_i$in the function $\tilde{\mathcal{Y}}$ The outcome yields a collection of n algebraic equations representing the unidentified constants Π_i. The subsequent subsections provide an explanation of three different ways of Weighted Residual Methods.

5.1 Collocation Method

In this approach, the weighting functions are derived from a set of Dirac δ functions within the given domain, that is $\widetilde{\mathrm{w}}_i = (\xi) = \delta(\xi - \xi_i)$ .The Dirac δ function is formally defined as

$$\widetilde{\mathrm{w}}_i = \delta(\xi - \xi_i) = \begin{cases} 1 & if\ \ \xi = \xi_i \\ 0 & \text{Otherwise} \end{cases} \tag{34}$$

The residual function in Eq. (32) needs to be constrained to zero at some points. In the context of this problem, a trial function is seen in Eq. (29). The trial function shown above fulfils the boundary condition as stated in Eq. (17), we obtain that,

$$\Pi_0 = 1, \tag{35}$$

$$\Pi_1 = -(2\Pi_2 + 3\Pi_3 + 4\Pi_4 + 5\Pi_5 + 6\Pi_6)\ , \tag{36}$$

By substituting the Eq. (35) and Eq. (36) into Eq. (29) we get that,

$$\tilde{\mathcal{Y}}(\xi) = 1 - \ (2\Pi_2 + 3\Pi_3 + 4\Pi_4 + 5\Pi_5 + 6\Pi_6)\xi^2 + \Pi_2\xi^4 + \Pi_3\xi^6 + \Pi_4\xi^8 + \Pi_5\xi^5\ . \tag{37}$$

The residual functions can be obtained by substituting Eq. (37) into Eq. (16), and denoted as $\mathcal{R}(\Pi_0, \Pi_1, \Pi_2, \Pi_3, \Pi_4, \Pi_5, \xi\ )$ may be determined,

$$\begin{aligned}\mathcal{R}(\Pi_0, \Pi_1, \Pi_2, \Pi_3, \Pi_4, \Pi_5) = &\left(1\ + \frac{1}{\gamma}\right)(720\xi^7\Pi_5 + \ 336\xi^5\Pi_4 + \ 120\xi^3\Pi_3 + \ 24\xi\Pi_2) + 2\varepsilon\mathrm{R}(\xi^{10}\Pi_5 \\ &+\xi^8\Pi_4 + \ \xi^6\Pi_3 + \xi^4\Pi_2 + \xi^2\Pi_1 + \ \Pi_1)(10\xi^9\Pi_5 + \ 8\xi^7\Pi_4 + \ 6\xi^5\Pi_3 + \ 4\xi^3\Pi_2 + \ 2\xi\Pi_1) \\ &+\varepsilon^2\left(4 + \frac{4}{\gamma} - H\right)(10\xi^9\Pi_5 + \ 8\xi^7\Pi_4 + \ 6\xi^5\Pi_3 \ + \ 4\xi^3\Pi_2 + 2\xi\Pi_1).\end{aligned} \tag{38}$$

However, the residual function must approximate zero. In order to achieve this objective, it is necessary to select four distinct locations inside the domain $\xi_i \in [0,1]$. Ultimately, after substituting these points into the residual function, $\mathcal{R}(\Pi_0, \Pi_1, \Pi_2, \Pi_3, \Pi_4, \Pi_5)$, a system of four equations and four unknown coefficients was derived. Once the unknown parameters $(\Pi_2, \Pi_3, \Pi_4, \Pi_5)$ are determined, they will be substituted into Eq. (37) to obtain the approximate solution.

5.2 The Sub-domain Collocation Method

This is an alternative method that can be employed to compute the parameters $\Pi_i, 0,1,2, \ldots, n$ The domain is partitioned into n subdomains, where

$$\overline{\mathrm{w}}_i = \begin{cases} 1 & if\ \ \xi_i \le \xi \le \xi_{i+1} \\ 0 & \text{Otherwise} \end{cases}. \tag{39}$$

This approach aims to reduce the residual error in each of the selected subdomains. Thus, Eq. (16) is fulfilled within every sub-domain, there by resulting in the transformation of Eq. (38).

$$\int_a^b \overline{\mathrm{w}}_i R(\xi)\, d\xi = \int_{\xi_i}^{\xi_{i+1}} R(\xi)\, d\xi = \ 0\ \text{, for } i = 1,2, \ldots . n \tag{40}$$

The trial function must satisfy the boundary condition specified in Eq. (17), and will be considered as the function defined in Eq. (37). The residual will be denoted by Eq. (38). By substituting the residual function, represented as $\mathcal{R}(\Pi_0, \Pi_1, \Pi_2, \Pi_3, \Pi_4, \Pi_5, \xi)$ into Eq. (40), a set of four equations will be derived. Solving this set of equations will allow for the derivation of the coefficients Π_2, Π_3, Π_4 and Π_5.

It should be noted that the sub-domains can be chosen at will. In many circumstances, dividing the complete domain evenly is the best option. However, if a higher resolution in a specific area is needed, a non-uniform choice may be preferable.

5.3 Least Square Method

The rationale for the name becomes apparent when the objective of minimizing the sum of squared residuals is considered. Put simply, a minimum of

$$\mathcal{G} = \int_a^b \mathcal{R}(\xi)\mathcal{R}(\xi)\, d\xi = \int_a^b \mathcal{R}^2(\xi)\, d\xi. \tag{41}$$

To attain the minimal value of this scalar function, it is necessary for the derivatives of the function with respect to all the unknown parameters to be equal to zero. That is to say:

$$\frac{\partial \mathcal{G}}{\partial \Pi_i} = 2\int_a^b \mathcal{R}(\xi)\frac{\partial \mathcal{R}}{\partial \Pi_i} d\xi = 0. \tag{42}$$

Upon comparison with Eq. (33), it is evident that the weight functions show the following characteristics:

$$\overline{\mathrm{w}}_i = 2\frac{\partial \mathcal{R}}{\partial \Pi_i}, \tag{43}$$

nevertheless, the coefficient of 2 can be omitted as it nullifies within the equation. Hence, the weight functions utilized in the Least Squares Method (LSM) correspond to the derivatives of the residual in relation to the unknown constants.

$$\overline{\mathrm{w}}_i = \frac{\partial \mathcal{R}}{\partial \Pi_i}. \tag{44}$$

The trial function must adhere to the boundary condition stated in Eq. (17), so it will be regarded as the function described in Eq. (37), and the residual will be represented by Eq. (38). By putting the residual function, denoted as $\mathcal{R}(\Pi_0, \Pi_1, \Pi_2, \Pi_3, \Pi_4, \Pi_5, \xi)$ into Eq. (42), a system of four equations will be obtained, solving this system of equations will enable the determination of the coefficients Π_2, Π_3, Π_4 and Π_5.

5.4 Galerkin Method

This method can be perceived as a variant of the Least Squares Method (LSM). Instead of employing the derivative of the residual with regard to the unknown Π_i,the derivative of the approximation function or trial function is utilized. Weight functions are utilized in this methodology,

$$\overline{\mathrm{w}}_i = \frac{\partial \tilde{y}}{\partial \Pi_i}\ , i = 1,2, \dots, n. \tag{45}$$

Firstly, as previously stated, let us consider the trial function denoted as Eq. (29) that fulfills the specified boundary condition outlined in Eq. (17). The weight functions can be derived by utilizing Eq. (45), it is possible to establish a collection of algebraic equations. Subsequently, the process of solving this set of equations yields the coefficients $\Pi_2, \Pi_3, \Pi_4, \Pi_5$. The approximate solution will be derived by substituting them into Eq. (37).

6. Convergence Test

In this section, the convergence of the analytical approximate solutions from the implementation of DTM for the nonlinear ordinary differential equations is discussed, and the derivation of the convergence condition to test the resulting solutions obtained by this technique, in the form of power series have been analysed. To study the convergence of the analytical approximate solutions, we presented some relevant theorem as follows:

Theorem [44]: Let $\tilde{\mathcal{P}}$ be an operator from a Hilbert space $\mathcal{H}_0$ into $\mathcal{H}_0$ and let $\mathcal{W}$ be an exact solution of Equation (16) ,then $\sum_{\mathrm{k}=0}^{\infty} \mathcal{W}(\mathrm{k})\xi^{\mathrm{k}}$ which is obtained by Eq. (21), converges to the exact solution, if there exists $0 \leq \pi < 1$ such that $\|\mathcal{W}_{\bar{k}+1}\| \leq \pi\|\mathcal{W}_{\bar{k}}\|\ \forall \bar{k} \in \mathrm{N} \cup \{0\}$

Proof: We have

$$\begin{aligned}
&\tilde{\mathrm{S}}_0 = 0\\
&\tilde{\mathrm{S}}_1 = \tilde{\mathrm{S}}_{1_0} + \mathcal{W}_1 = \mathcal{W}_1.\\
&\tilde{\mathrm{S}}_2 = \tilde{\mathrm{S}}_1 + \mathcal{W}_2 = \mathcal{W}_1 + \mathcal{W}_2.\\
&\vdots\\
&\tilde{\mathrm{S}}_{\mathrm{n}} = \tilde{\mathrm{S}}_{\mathrm{n}-1} + \mathcal{W}_{\mathrm{n}} = \mathcal{W}_1 + \mathcal{W}_2 + \cdots + \mathcal{W}_{\mathrm{n}}.
\end{aligned}$$

We will demonstrate that the sequence $\left\{\tilde{\mathrm{S}}_{\mathrm{n}}\right\}_{n=0}^{\infty}$ is a Cauchy sequence in the Hilbert Space $\mathcal{H}_0$.

Now for

$$\left\|\tilde{\mathrm{S}}_{\mathrm{n}+1} - \tilde{\mathrm{S}}_{\mathrm{n}}\right\| = \|\mathcal{W}_{\mathrm{n}+1}\| \leq \pi\|\mathcal{W}_{\mathrm{n}}\| \leq \pi^2\|\mathcal{W}_{\mathrm{n}-1}\| + \cdots \leq \pi^{\mathrm{n}}\|\mathcal{W}_0\|$$

For any natural numbers n and m, $n \geq m$ we have,

$$\begin{aligned}
&\left\|\tilde{\mathrm{S}}_{\mathrm{n}} - \tilde{\mathrm{S}}_{\mathrm{m}}\right\| = \left\|\left(\tilde{\mathrm{S}}_{\mathrm{n}} - \tilde{\mathrm{S}}_{\mathrm{n}-1}\right) + \left(\tilde{\mathrm{S}}_{\mathrm{n}-1} - \tilde{\mathrm{S}}_{\mathrm{n}-2}\right) + \cdots \left(\tilde{\mathrm{S}}_{\mathrm{m}-2} - \tilde{\mathrm{S}}_{\mathrm{m}+1}\right) + \left(\tilde{\mathrm{S}}_{\mathrm{m}+1} - \tilde{\mathrm{S}}_{\mathrm{m}}\right)\right\| \leq \left\|\tilde{\mathrm{S}}_{\mathrm{n}} - \tilde{\mathrm{S}}_{\mathrm{n}-1}\right\|\\
&+\left\|\tilde{\mathrm{S}}_{\mathrm{n}-1} - \tilde{\mathrm{S}}_{\mathrm{n}-2}\right\| + \cdots \left\|\tilde{\mathrm{S}}_{\mathrm{m}-2} - \tilde{S}_{\mathrm{m}+1}\right\| + \left\|\tilde{S}_{\mathrm{m}+1} - \tilde{S}_{\mathrm{m}}\right\| \leq \pi^{\mathrm{n}}\|\mathcal{W}_0\| + \pi^{\mathrm{n}-1}\|\mathcal{W}_0\| + \pi^{\mathrm{n}-2}\|\mathcal{W}_0\| +\\
&+\pi^{\mathrm{n}-3}\|\mathcal{W}_0\| + \cdots + \pi^{\mathrm{m}+2}\|\mathcal{W}_0\| + \pi^{\mathrm{m}+1}\|\mathcal{W}_0\| \leq (\pi^{\mathrm{m}+1} + \pi^{\mathrm{m}+2} + \cdots)\|\mathcal{W}_0\| = \frac{\pi^{\mathrm{m}+1}}{(1-\pi)}\|\mathcal{W}_0\|.
\end{aligned}$$

It may be inferred that $\lim_{n,m\to\infty} \left\|\tilde{\mathrm{S}}_{\mathrm{n}} - \tilde{\mathrm{S}}_{\mathrm{m}}\right\| = 0$, meaning $\{S_n\}_{n=0}^{\infty}$ is a Cauchy sequence in the Hilbert space $\mathcal{H}$ and it converges to $\tilde{\mathrm{S}}$ for any $\tilde{\mathrm{S}} \in \mathcal{H}$. From theorem can be determined the convergence of DTM through introduce the convergence condition in the following definition and corollary.

Definition [44]: For every $j \in \mathrm{N} \cup \{0\}$, π_j can be defined as

$$\pi_j = \begin{cases} \dfrac{\|\mathcal{W}_{j+1}\|}{\|\mathcal{W}_j\|} & \|\mathcal{W}_j\| \neq 0 \\ 0 & \|\mathcal{W}_j\| = 0 \end{cases}.$$

Corollary [33]: If $0 \leq \pi_j < 1$, $j = 1.2, \ldots$, then $\sum_{k=0}^{\infty} \mathcal{W}_j$ is converges to the exact solution $\mathcal{W}$.

According to apply the condition of convergence in definition with L_∞-norm to find the convergence of the solutions of DTM. Since $\pi_0 = \frac{\|\mathcal{W}_1\|}{\|\mathcal{W}_0\|} = 0 < 1$, $\pi_1 = \frac{\|\mathcal{W}_2\|}{\|\mathcal{W}_1\|} = 0 < 1$, $\pi_2 = \frac{\|\mathcal{W}_3\|}{\|\mathcal{W}_2\|} = 0 < 1$, ….. In a similar manner, $\pi_j = 0$ for all j . All solutions are achieved for the corollary, therefore $\mathcal{Y}(\xi) = \sum_{k=0}^{\infty} \mathcal{W}(k)\xi^{\bar{k}}$ is convergent.

7. Discuss Tabular

The impacts of many physical parameters, such as the Reynolds number R_e, Casson fluid parameter γ, Hartmann number H_a, open-angles ε, and stretching shrinking parameter $\bar{\chi}$ on velocity profile $\mathcal{Y}(\xi)$ are the objective of our study by applying the differential transform method and the optimal differential transform method to get an analytical solution of magneto-hydrodynamic Jeffery Hamel flow of Casson fluid problem. A comparison is made between the outcomes achieved using the optimal differential transform method for divergent and convergent channels and the outcomes acquired through the differential transform method can be display in the following tables. Table 2 to Table 4 given a comparison of the findings of DTM, CDTM, SDTM, LSDTM, and GDTM with the numerical solution by the BVP4c, this demonstrates a strong concurrence between DTM and ODTMs finding and the existing numerical solution.

Table 2
Comparison between BVP4c, DTM, CDTM, SDTM, LSDTM and GDTM for $R_e = 5$, $H = 100, \gamma = 0.2$, $\bar{\chi} = 0.1$ and $\varepsilon = 3^{\circ}$

ξ	BVP4	DTM	CDTM	SDTM	LDTM	GDTM
0.0	1.0000000000	1.0000000000	1.0000000000	1.0000000000	1.0000000000	1.0000000000
0.1	0.9909727360	0.9909727361	0.9909727360	0.9909727360	0.9909727360	0.9909727360
0.2	0.9638956138	0.9638956141	0.9638956139	0.9638956139	0.9638956139	0.9638956139
0.3	0.9187822147	0.9187822154	0.9187822148	0.9187822147	0.9187822148	0.9187822147
0.4	0.8556537472	0.8556537483	0.8556537473	0.8556537472	0.8556537473	0.8556537472
0.5	0.7745369116	0.7745369134	0.7745369116	0.7745369116	0.7745369116	0.7745369116
0.6	0.6754609174	0.6754609199	0.6754609174	0.6754609174	0.6754609174	0.6754609174
0.7	0.5584536616	0.5584536650	0.5584536616	0.5584536616	0.5584536616	0.5584536616
0.8	0.4235370716	0.4235370757	0.4235370717	0.4235370717	0.4235370717	0.4235370717
0.9	0.2707216188	0.2707216226	0.2707216188	0.2707216188	0.2707216188	0.2707216188
1.0	0.1000000000	0.10000000000	0.1000000000	0.1000000000	0.1000000000	0.1000000000

Table 3
Comparison between BVP4c, DTM, CDTM, SDTM, LSDTM and GDTM for $R_e = 5$, $H = 100, \gamma = 0.2$, $\bar{\chi} = 0.1$ and $\varepsilon = 3^{\circ}$

ξ	BVP4	DTM	CDTM	SDTM	LDTM	GDTM
0.0	1.0000000000	1.0000000000	1.0000000000	1.0000000000	1.0000000000	1.0000000000
0.1	0.9920710131	0.9920710130	0.9920710131	0.9920710131	0.9920710131	0.9920710131
0.2	0.9682743201	0.9682743196	0.9682743201	0.9682743201	0.9682743201	0.9682743201
0.3	0.9285810717	0.9285810705	0.9285810718	0.9285810718	0.9285810717	0.9285810717
0.4	0.8729443465	0.8729443443	0.8729443465	0.8729443466	0.8729443465	0.8729443464
0.5	0.8013009006	0.8013008972	0.8013009007	0.8013009007	0.8013009006	0.8013009005
0.6	0.7135736356	0.7135736307	0.7135736357	0.7135736358	0.7135736357	0.7135736356
0.7	0.6096747993	0.6096747929	0.6096747994	0.6096747995	0.6096747994	0.6096747993
0.8	0.4895099396	0.4895099317	0.4895099396	0.4895099398	0.4895099396	0.4895099395
0.9	0.3529826316	0.3529826242	0.3529826318	0.3529826319	0.3529826317	0.3529826316
1.0	0.2000000000	0.2000000000	0.2000000000	0.2000000000	0.2000000000	0.2000000000

Table 4
Comparison between BVP4c, DTM, CDTM, SDTM, LSDTM and GDTM for $R_e = 5$, $H = 100, \gamma = 0.2$, $\bar{\chi} = 0.1$ and $\varepsilon = 3^{\circ}$

ξ	BVP4	DTM	CDTM	SDTM	LDTM	GDTM
0.0	1.0000000000	1.0000000000	1.0000000000	1.0000000000	1.0000000000	1.0000000000
0.1	0.9889739061	0.9889739062	0.9889739061	0.9889739061	0.9889739061	0.9889739061
0.2	0.9559006661	0.9559006665	0.9559006662	0.9559006662	0.9559006662	0.9559006662
0.3	0.9007948160	0.9007948168	0.9007948160	0.9007948160	0.9007948160	0.9007948161
0.4	0.8236786197	0.8236786211	0.8236786197	0.8236786197	0.8236786197	0.8236786198
0.5	0.7245791309	0.7245791331	0.7245791309	0.7245791309	0.7245791309	0.7245791310
0.6	0.6035240883	0.6035240915	0.6035240883	0.6035240883	0.6035240883	0.6035240883
0.7	0.4605366510	0.4605366552	0.4605366510	0.4605366509	0.4605366510	0.4605366510
0.8	0.2956289802	0.2956289853	0.2956289802	0.2956289801	0.2956289802	0.2956289802
0.9	0.1087946669	0.1087946715	0.1087946669	0.1087946668	0.1087946669	0.1087946669
1.0	-0.1000000000	-0.1000000000	-0.1000000000	-0.1000000000	-0.1000000000	-0.1000000000

Also, the error of percentage was derived in Table 5 to Table 7. From these tables it can be seen that CDTM, SDTM, LSDTM, and GDTM have higher accuracy than DTM.

Table 5
Comparison between the error of BVP4c, DTM, CDTM, SDTM, LSDTM and GDTM for $R_e = 10$, $H_a = 500, \gamma = 0.4$, $\bar{\chi} = -0.1$ and $\varepsilon = 1^{\circ}$

ξ	DTM	CDTM	SDTM	LDTM	GDTM
0.0	0.000000000	0.000000000	0.000000000	0.000000000	0.000000000
0.1	2.02×10^{-10}	0.000000000	0.000000000	1.01×10^{-10}	1.01×10^{-10}
0.2	7.32×10^{-10}	0.000000000	0.000000000	1.04×10^{-10}	1.04×10^{-10}
0.3	1.77×10^{-9}	0.000000000	0.000000000	1.11×10^{-10}	2.22×10^{-10}
0.4	3.27×10^{-9}	0.000000000	0.000000000	1.21×10^{-10}	1.21×10^{-10}
0.5	5.93×10^{-9}	0.000000000	0.000000000	1.38×10^{-10}	2.76×10^{-10}
0.6	1.01×10^{-8}	0.000000000	1.65×10^{-10}	0.000000000	1.65×10^{-10}
0.7	1.73×10^{-8}	0.000000000	2.17×10^{-10}	0.000000000	2.17×10^{-10}
0.8	3.21×10^{-8}	3.38×10^{-10}	6.76×10^{-10}	0.000000000	0.000000000
0.9	8.09×10^{-8}	9.19×10^{-10}	1.83×10^{-10}	0.000000000	0.000000000
1.0	0.000000000	0.000000000	0.000000000	0.000000000	0.000000000

Table 6
Comparison between the error of BVP4c, DTM, CDTM, SDTM, LSDTM and GDTM for $R_e = 20$, $H = 300, \gamma = 0.1$, $\bar{\chi} = 0$ and $\varepsilon = -2^{\circ}$

ξ	DTM	CDTM	SDTM	LDTM	GDTM
0.0	0.000000000	0.000000000	0.000000000	0.000000000	0.000000000
0.1	5.04×10^{-10}	0.000000000	0.000000000	0.000000000	2.08×10^{-10}
0.2	2.39×10^{-9}	0.000000000	1.04×10^{-10}	2.08×10^{-10}	4.39×10^{-10}
0.3	5.70×10^{-9}	0.000000000	1.09×10^{-10}	4.39×10^{-10}	4.75×10^{-10}
0.4	1.09×10^{-8}	1.18×10^{-10}	2.37×10^{-10}	3.56×10^{-10}	5.31×10^{-10}
0.5	1.91×10^{-8}	1.32×10^{-10}	3.98×10^{-10}	1.32×10^{-10}	4.67×10^{-10}
0.6	3.20×10^{-8}	0.000000000	6.22×10^{-10}	0.000000000	5.85×10^{-10}
0.7	5.36×10^{-8}	0.000000000	1.17×10^{-9}	0.000000000	8.28×10^{-10}
0.8	9.11×10^{-8}	2.76×10^{-10}	2.48×10^{-9}	0.000000000	5.22×10^{-10}
0.9	1.5×10^{-7}	1.56×10^{-10}	4.70×10^{-9}	5.22×10^{-10}	2.08×10^{-10}
1.0	0.000000000	0.000000000	0.000000000	0.000000000	0.000000000

Table 7
Comparison between the error of BVP4c, DTM, CDTM, SDTM, LSDTM and GDTM for $R_e = 10$, $H = 200, \gamma = 0.2$, $\bar{\chi} = 0.1$ and $\varepsilon = 3^{\circ}$

ξ	DTM	CDTM	SDTM	LDTM	GDTM
0.0	0.000000000	0.000000000	0.000000000	0.000000000	0.000000000
0.1	4.03×10^{-10}	0.000000000	0.000000000	0.000000000	0.000000000
0.2	1.97×10^{-9}	0.000000000	0.000000000	1.03×10^{-10}	2.07×10^{-10}
0.3	4.57×10^{-9}	0.000000000	1.08×10^{-10}	1.08×10^{-10}	2.17×10^{-10}
0.4	8.88×10^{-9}	0.000000000	1.16×10^{-10}	2.33×10^{-10}	3.50×10^{-10}
0.5	1.52×10^{-8}	0.000000000	1.29×10^{-10}	1.29×10^{-10}	3.87×10^{-10}
0.6	2.48×10^{-8}	1.48×10^{-10}	4.44×10^{-10}	1.48×10^{-10}	2.96×10^{-10}
0.7	4.03×10^{-8}	0.000000000	5.37×10^{-10}	0.000000000	3.58×10^{-10}
0.8	6.33×10^{-8}	2.36×10^{-10}	1.41×10^{-10}	0.000000000	2.36×10^{-10}
0.9	9.01×10^{-8}	7.39×10^{-10}	2.21×10^{-10}	0.000000000	0.000000000
1.0	0.000000000	0.000000000	0.000000000	0.000000000	0.000000000

In Table 8 to Table 10 evaluated the solutions of $\frac{d^2y(0)}{d\xi^2}$ acquired through DTM, CDTM, SDTM, LSDTM, and GDTM, and compare them with the numerical solution obtained using BVP4c. Theses tables displayed that the outcomes of the collocation differential transform method (CDTM), the sub-domain differential transform method (SDTM), the least squares differential transform method (LSDTM), and the Galerkin differential transform method (GDTM) are more convergent to the numerical solution from the results of differential transform method (DTM).

Table 8
The convergent of $\frac{d^2y(0)}{d\xi^2}$ between BVP4c, DTM, CDTM, SDTM, LDTM, and GDTM

γ	BVP4c	DTM	CDTM	SDTM	LDTM	GDTM
0.1	-1.60347128	-1.60347193	-1.60347193	-1.60347193	-1.60347193	-1.60347193
0.2	-1.60515038	-1.60515037	-1.60515038	-1.60515038	-1.60515038	-1.60515038
0.3	-1.60657170	-1.60657169	-1.60657170	-1.60657170	-1.60657170	-1.60657170
0.4	-1.60779076	-1.60779072	-1.60779076	-1.60779076	-1.60779076	-1.60779076

Table 9

The convergent of $\frac{d^2y(0)}{d\xi^2}$ between BVP4c, DTM, CDTM, SDTM, LDTM, and GDTM

H	BVP4c	DTM	CDTM	SDTM	LDTM	GDTM
0.00	-1.81450763	-1.81450758	-1.81450763	-1.81450763	-1.81450763	-1.81450763
400	-1.80841163	-1.80841160	-1.808411638	-1.80841163	-1.80841163	-1.80841163
500	-1.80689147	-1.80689144	-1.80689147	-1.80689147	-1.80689147	-1.80689147
600	-1.80537284	-1.80537282	-1.80537284	-1.80537284	-1.80537284	-1.80537284

Table 10

The convergent of $\frac{d^2y(0)}{d\xi^2}$ between BVP4c, DTM, CDTM, SDTM, LDTM, and GDTM

$\bar{\chi}$	BVP4c	DTM	CDTM	SDTM	LDTM	GDTM
-0.2	-2.40851794	-2.40851786	-2.40851794	-2.4085179	-2.40851794	-2.40851794
0.0	-2.00787701	-2.00787697	-2.00787701	-2.0078770	-2.00787701	-2.00787701
0.2	-1.60692524	-1.60692521	-1.60692524	-1.6069252	-1.60692524	-1.60692524
0.4	-1.20566213	-1.20566212	-1.20566213	-1.2056621	-1.20566213	-1.20566213

Table 11 shows the observed convergence of values Π exhibits uniformity in decimal places and stays invariant when the iterative approaches are extended.

Table 11

The convergence of values Π

Approximate Order	$R_e = 10$,$\gamma = 0.3$, $H_a = 100$ and $\bar{\chi} = 0.3$		$R_e = 10$,$\gamma = 0.1$, $H_a = 100$ and $\bar{\chi} = 0.1$	
	$\varepsilon = 1^{\circ}$	$\varepsilon = -1^{\circ}$	$\varepsilon = 3^{\circ}$	$\varepsilon = -3^{\circ}$
Order10	−0.9045167866	−0.8946440778	−0.9048159700	−0.8931344988
Order11	−0.9045167866	−0.8946440778	−0.9048159700	−0.8931344988
Order12	−0.9045176974	−0.8946440778	−0.9048159840	−0.8931344813
Order13	−0.9045176974	−0.8946440778	−0.9048159840	−0.8931344813
Order14	−0.904516 7866	−0.8946440684	−0.9048159829	−0.8931344821
Order15	−0.9045167866	−0.8946440684	−0.9048159829	−0.8931344821
Order16	−0.9045167859	−0.8946440684	−0.9048159828	−0.8931344821
Order17	−0.9045167859	−0.8946440684	−0.9048159828	−0.8931344821
Order18	−0.9045167859	−0.8946440684	−0.9048159828	−0.8931344821
Order19	−0.9045167859	−0.8946440684	−0.9048159828	−0.8931344821
Order20	−0.9045167859	−0.8946440684	−0.9048159828	−0.8931344821

8. Discuss Graphics

(i) Graphics show the effect of Reynolds number R_e on the velocity $\mathcal{Y}(\xi)$

The impact of the Reynolds number R_e on the velocity profile $\mathcal{Y}(\xi)$ is seen in Figure 3 to Figure 6. The presented figures illustrate a positive correlation between the Reynolds number R_e and the reduction in fluid velocity in divergent channels undergoing stretching- shrinking. However, it is worth noting that there exists a contrasting pattern in stretching-shrinking convergent channels, where the velocity profile shows an increase as the Reynolds number increases.

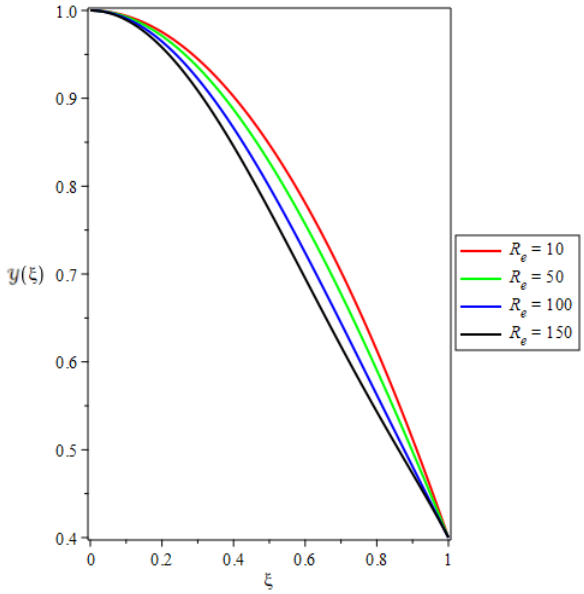

Fig. 3. Influence of variation of R_e, on the velocity $\mathcal{Y}(\xi)$ when $\gamma = 0.5$, $H_a = 100$, $\bar{\chi} = 0.8$ and $\varepsilon = 5^{\circ}$

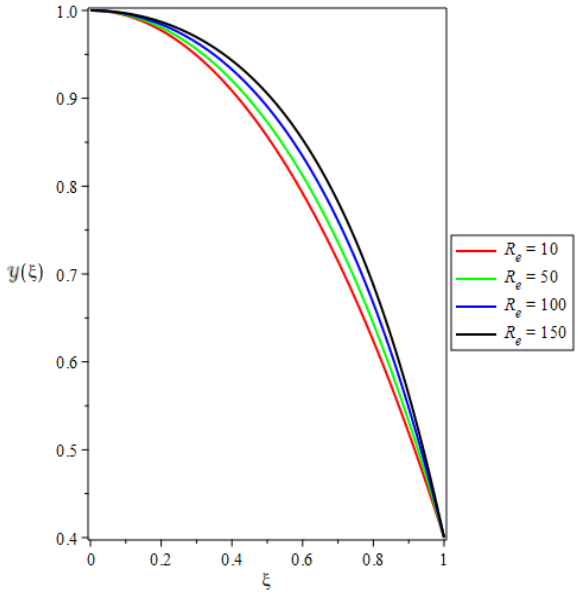

Fig. 4. Influence of variation of R_e, on the velocity $\mathcal{Y}(\xi)$ when $\gamma = 0.5$, $H_a = 100$, $\bar{\chi} = 0.8$ and $\varepsilon = -5^{\circ}$

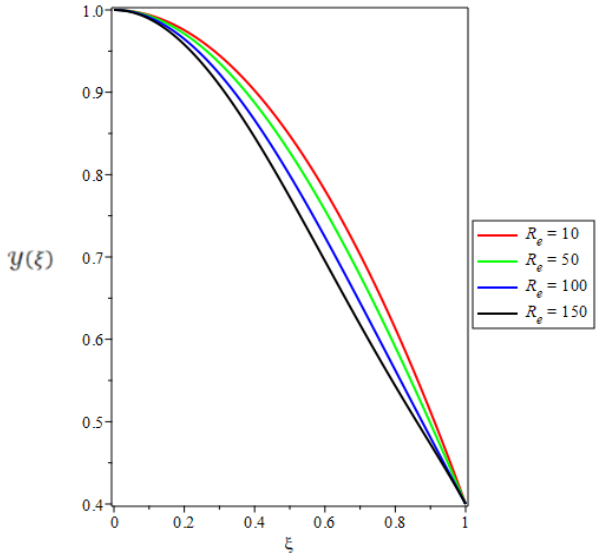

Fig. 5. Influence of variation of R_e,on the velocity $\mathcal{Y}(\xi)$ when $\gamma = 0.5$, $H_a = 100$, $\bar{\chi} = -0.8$ and $\varepsilon = 5^{\circ}$

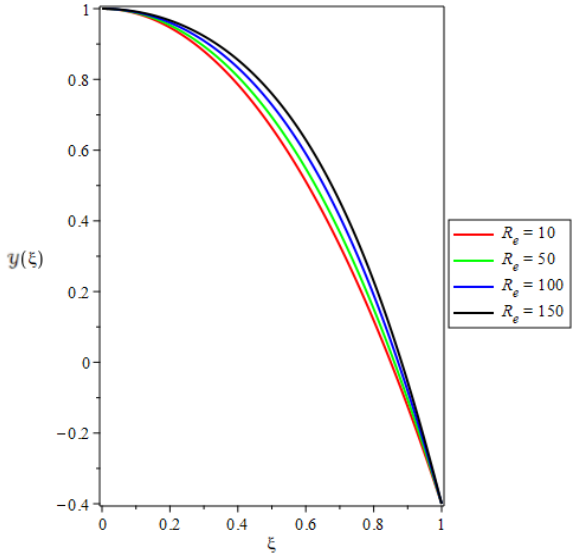

Fig. 6. Influence of variation of R_e,on the velocity $\mathcal{Y}(\xi)$ when $\gamma = 0.5$, $H_a = 100$, $\bar{\chi} = -0.8$ and $\varepsilon = -5^{\circ}$

(ii) Graphics show the effect of the angle ε on the velocity $\mathcal{Y}(\xi)$

Figure 7 to Figure 10 illustrate the relationship between the opening angle and the fluid velocity in divergent convergent channels that undergo stretching and shrinking. Based on the presented figures, it can be shown that the velocity profile exhibits a declining trend as a function of angle in the context of a stretching-shrinking divergent channel. Furthermore, the velocity profile exhibits an increase as the absolute values of the opening angle grow.

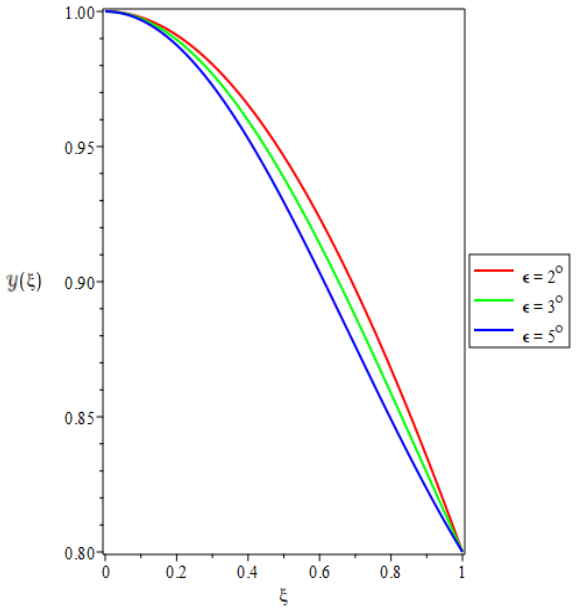

Fig. 7. Influence of variation of ε on the velocity $\mathcal{Y}(\xi)$ when $\gamma = 0.5$, $H_a = 100$, $\bar{\chi} = 0.8$ and $R_e = 100$

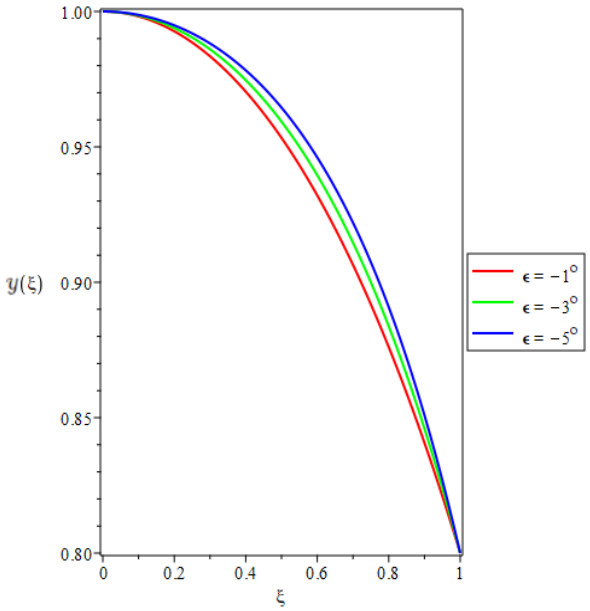

Fig. 8. Influence of variation of ε on the velocity $\mathcal{Y}(\xi)$ when $\gamma = 0.5$, $H_a = 100$, $\bar{\chi} = 0.8$ and $R_e = 100$

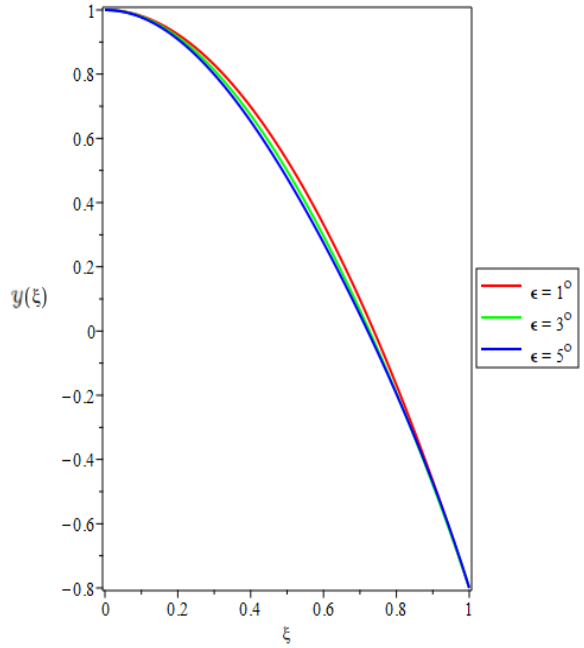

Fig. 9. Influence of variation of ε,on the velocity $\mathcal{Y}(\xi)$ when $\gamma = 0.5$, $H_a = 100$, $\bar{\chi} = -0.8$ and $R_e = 100$

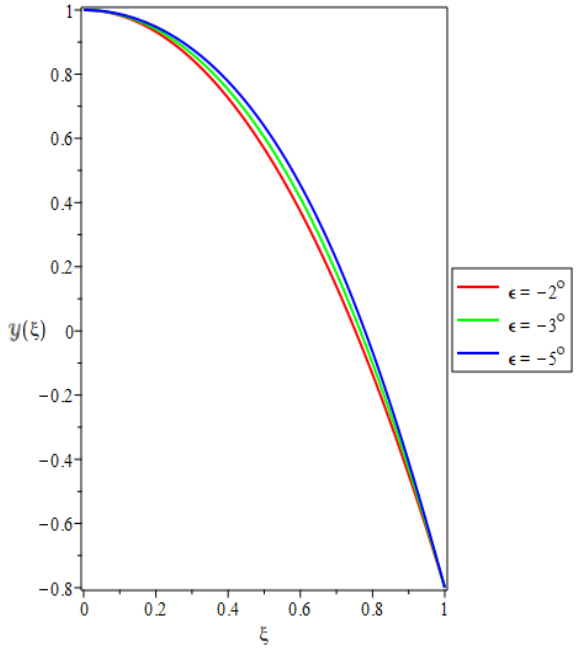

Fig. 10. Influence of variation of ε,on the velocity $\mathcal{Y}(\xi)$ when $\gamma = 0.5$, $H_a = 40$, $\bar{\chi} = -0.8$ and $R_e = 100$

(iii) Graphics show the effect of Casson fluid parameter γ on the velocity $\mathcal{Y}(\xi)$

Figure 11 to Figure 14 depict the impact of the Casson fluid parameter on the fluid velocity profiles inside the divergent and convergent channels, correspondingly. In the context of the diverging channel, it is seen that a rise in the Casson fluid parameter leads to a notable drop in the velocity profiles. In contrast, it can be shown from Figures that an increase in the Casson fluid parameter leads to a reduction in the velocity of fluid flow. It is anticipated that an augmentation in the Casson fluid

parameter is used to diminish the stress, which in turn augments the dynamic viscosity, thus generating a hindrance in the flow of the fluid.

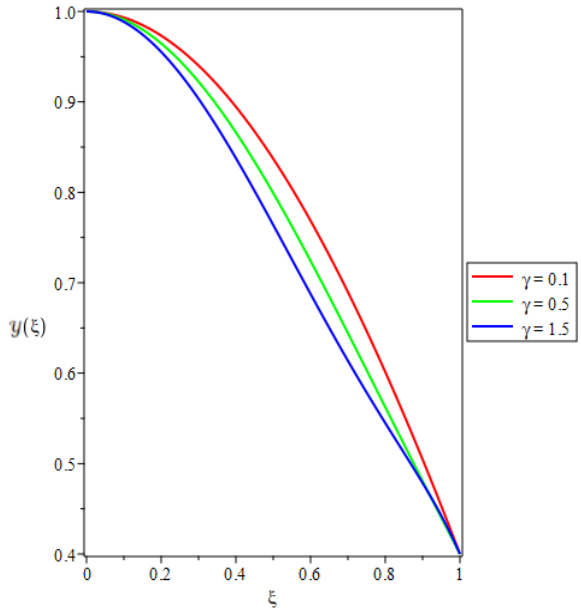

Fig. 11. Influence of variation of γ,on the velocity $\mathcal{Y}(\xi)$ when $R_e = 100$, $H_a = 100$, $\bar{\chi} = 0.8$ and $\varepsilon = 5^{\circ}$

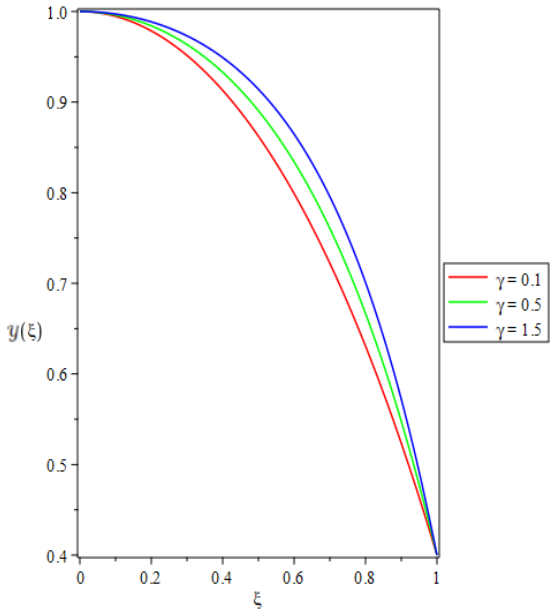

Fig. 12. Influence of variation of γ,on the velocity $\mathcal{Y}(\xi)$ when $R_e = 100$, $H_a = 100$, $\bar{\chi} = 0.8$ and $\varepsilon = -5^{\circ}$

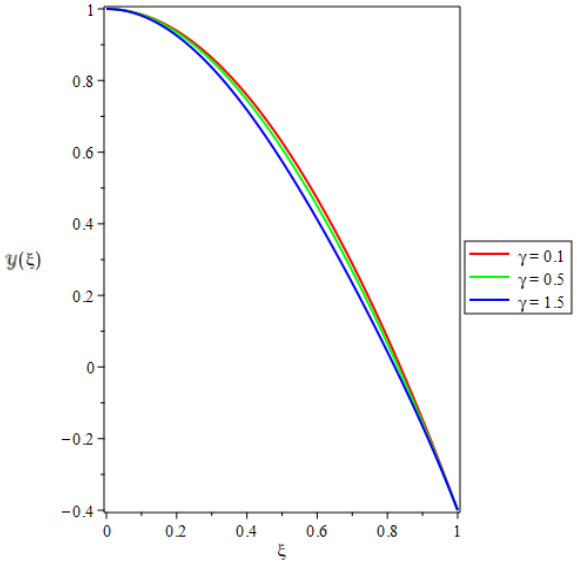

Fig. 13. Influence of variation of γ,on the velocity $\mathcal{Y}(\xi)$ when $R_e = 100$, $H_a = 100$, $\bar{\chi} = -0.8$ and $\varepsilon = 5^{\circ}$

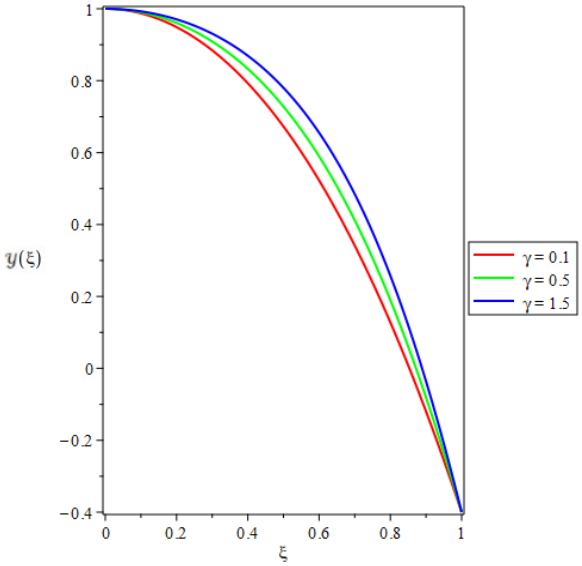

Fig. 14. Influence of variation of γ,on the velocity $\mathcal{Y}(\xi)$ when $R_e = 100$, $H_a = 100$, $\bar{\chi} = -0.8$ and $\varepsilon = -5^{\circ}$

(iv) Graphics show the effect of stretching-shrinking parameter $\bar{\chi}$ on the velocity $\mathcal{Y}(\xi)$

The presented Figure 15 to Figure 18 depict the impact of stretching-shrinking parameters on the velocity profiles within divergent-convergent channels. The analysis of these figures reveals that the velocity profiles exhibit an increase with the augmentation of the stretching parameter in stretching channels. Conversely, in the case of shrinking channels, the velocity profiles experience a decrease due to the amplification of the absolute value of shrinking.

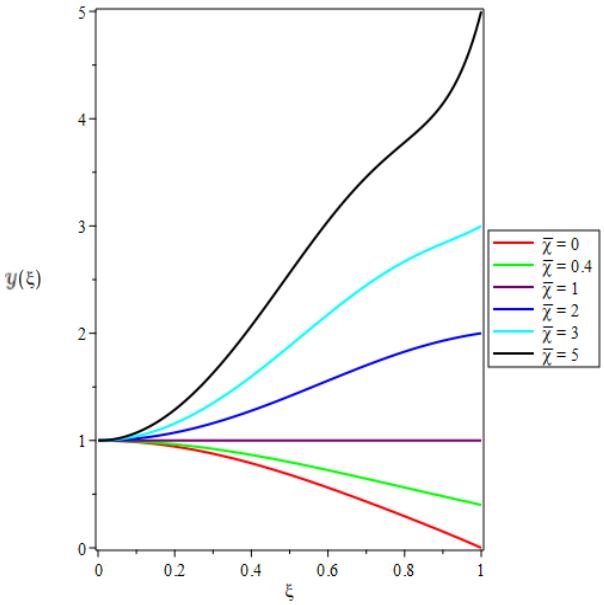

Fig. 15. Influence of variation of $\bar{\chi}$ on the velocity $\mathcal{Y}(\xi)$ when $\gamma = 0.5$, $H_a = 100$, $R_e = 100$ and $\varepsilon = 5^{\circ}$

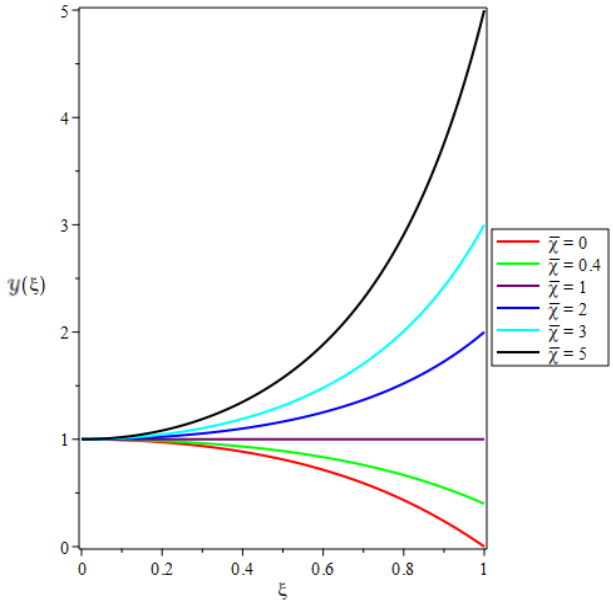

Fig. 16. Influence of variation of $\bar{\chi}$ on the velocity $\mathcal{Y}(\xi)$ when $\gamma = 0.5$, $H_a = 100$, $R_e = 100$ and $\varepsilon = -5^{\circ}$

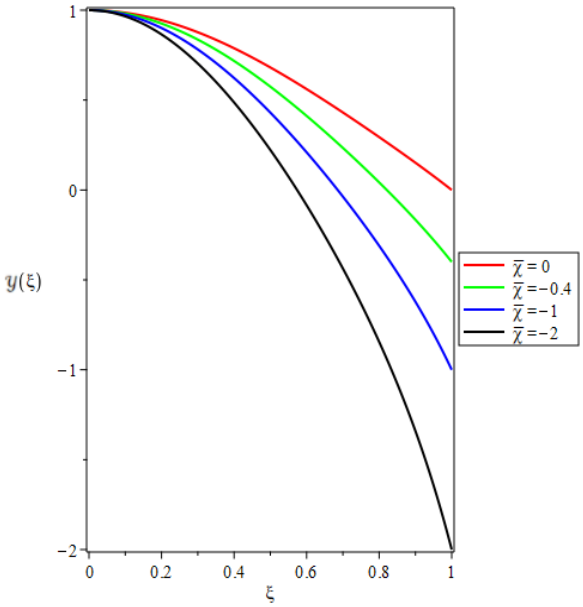

Fig. 17. Influence of variation of $\bar{\chi}$ on the velocity $\mathcal{Y}(\xi)$ when $\gamma = 0.5$, $H_a = 100$, $R_e = 100$ and $\varepsilon = 5^{\circ}$

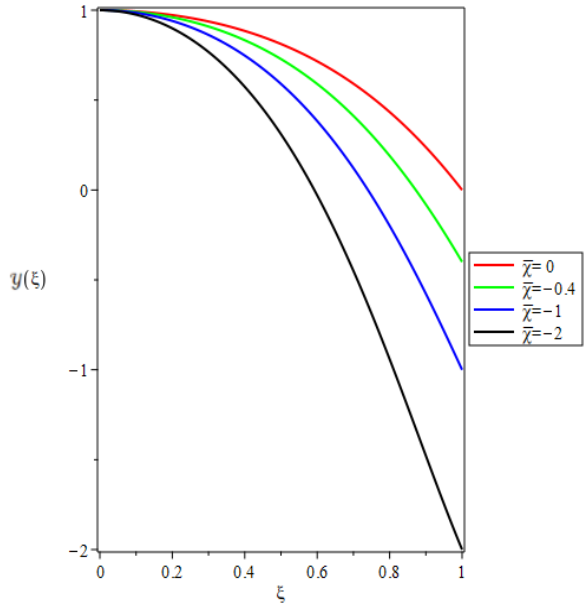

Fig. 18. Influence of variation of $\bar{\chi}$ on the velocity $\mathcal{Y}(\xi)$ when $\gamma = 0.5$, $H_a = 100$, $R_e = 100$ and $\varepsilon = -5^{\circ}$

(v) Graphics show the effect of the Hartmann number H_a on the velocity $\mathcal{Y}(\xi)$

Figure 19 to Figure 22 depicts the impact on the Hartmann number H_a of a velocity profile $\mathcal{Y}(\xi)$ within diverging-converging channels. The Hartmann number exhibits a notable correlation with the velocity profiles, as it grows in conjunction with the diverging and converging channel.

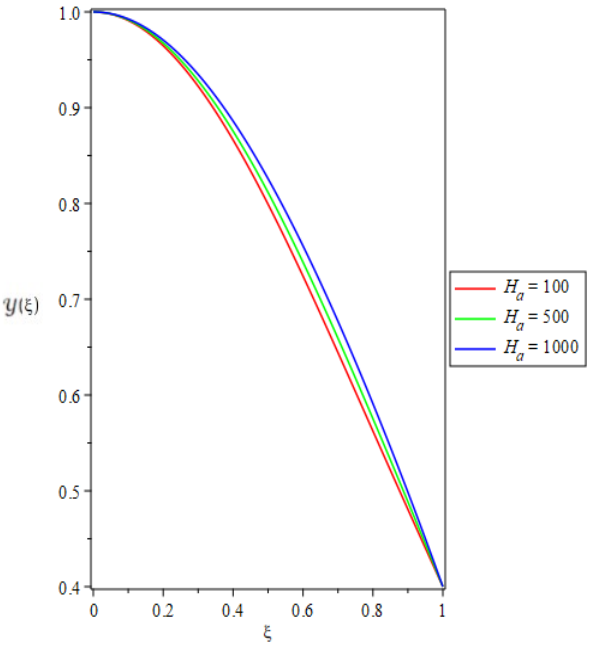

Fig. 19. Influence of variation of H_a on the velocity $\mathcal{Y}(\xi)$ when $\gamma = 0.5$, $\bar{\chi} = 0.8$, $R_e = 100$ and $\varepsilon = 5^{\circ}$

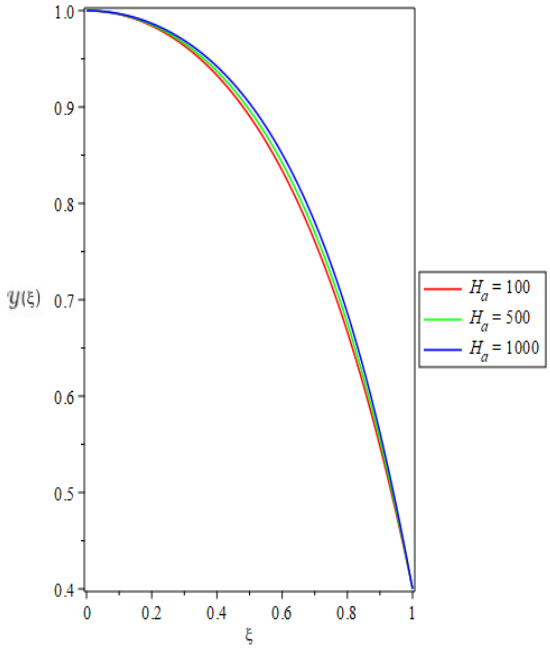

Fig. 20. Influence of variation of H_a on the velocity $\mathcal{Y}(\xi)$ when $\gamma = 0.5$, $\bar{\chi} = 0.8$, $R_e = 100$ and $\varepsilon = -5^{\circ}$

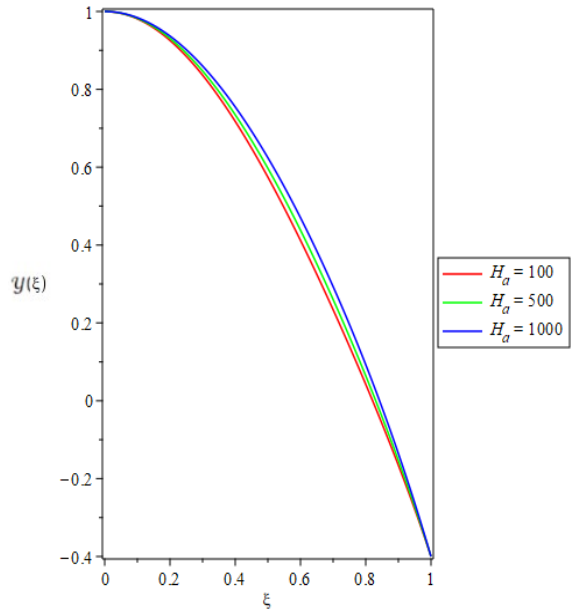

Fig. 21. Influence of variation of H_a on the velocity $\mathcal{Y}(\xi)$ when $\gamma = 0.5$, $\bar{\chi} = -0.8$, $R_e = 100$ and $\varepsilon = 5^{\circ}$

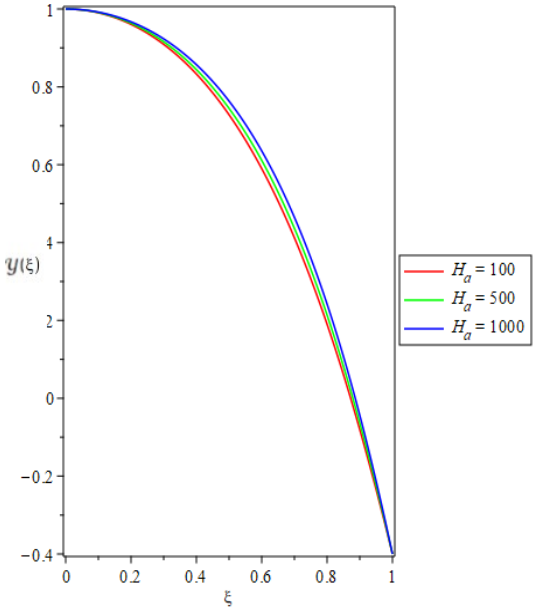

Fig. 22. Influence of variation of H_a on the velocity $\mathcal{Y}(\xi)$ when $\gamma = 0.5$, $\bar{\chi} = -0.8$, $R_e = 100$ and $\varepsilon = -5^{\circ}$

9. Conclusions

In this paper, the Jeffery-Hamel flow of non-Newtonian Casson fluid is introduced and afterwards addressed by the use of the Optimal differential transform method for analysing when the rise of physical parameters. The velocity behaviour in the expanding channel exhibited an opposing trend compared to that seen in the shrinking channel. The current study demonstrates a favourable agreement between the obtained findings of fixed values for the initial condition for various of the Casson fluid parameter, the Hartmann number and stretching-shrinking parameter. The comparison

demonstrates that the proportion of errors related with the Optimal differential transform method is much lower than that related to differential transform method. Based on our analysis, it can be inferred that the Optimal differential transform method exhibits more accuracy compared to the differential transform method. Consequently, the Optimal differential transform method may be considered a viable and efficient approximation semi-analytical technique for resolving the nonlinear equation governing the MHD Jeffery-Hamel flow of non-Newtonian Casson fluid. The observed nonlinearity in the velocity increase might likely be attributed to an increase in drag force exerted on the surface when the stretching parameter reaches higher levels. The important conclusions can be summed

(i) In diverging channel: There are two cases that can be explained in the case of stretching when the velocity reduces with the increase of the Reynolds number, the open angle, and the Casson fluid parameter, but there is a difference in the effect of the Hartmann number which is the opposite. In the case of shrinking, the velocity increases with increasing Reynolds number and Hartmann number but the effect of open angle and Casson fluid parameter is opposite.
(ii) In converging channel: The influence of the Reynolds number, the Casson fluid parameter and the Hartmann number in the cases of stretching and shrinking is similar, mean that the velocity profile increment with increasing these parameters. In addition, there is a difference in the behaviour of the open angle in both cases.

Acknowledgement
This research was not funded by any grant.

References

[1] Davidson, P. A., and Elena V. Belova. "An Introduction to Magnetohydrodynamics." *American Journal of Physics* 70, no. 7 (2002): 781-781. https://doi.org/10.1119/1.1482065
[2] Rehman, Sohail, Youssef Trabelsi, Sultan Alqahtani, Sultan Alshehery, and Sayed M. Eldin. "A renovated Jaffrey-Hamel flow problem and new scaling statistics for heat, mass fluxes with Cattaneo-Christov heat flux model." *Case Studies in Thermal Engineering* 43 (2023): 102787. https://doi.org/10.1016/j.csite.2023.102787
[3] Rehman, Sohail, Fuad AM Al-Yarimi, Sultan Alqahtani, and Mohammed Awad. "Dissipative flow features of Carreau nanofluid with thermal radiation inside plane wall channel: Jeffery-Hamel analysis." *Propulsion and Power Research* 12, no. 2 (2023): 253-272. https://doi.org/10.1016/j.jppr.2023.02.007
[4] Rehman, Sohail, Fahad S. Almubaddel, Y. M. Mahrous, Fares A. Alsadoun, and Amr S. Abouzied. "A generalization of Jeffrey-Hamel problem to Reiner-Rivlin model for energy and thermodynamic analysis using Keller-Box computational framework." *Case Studies in Thermal Engineering* 50 (2023): 103462. https://doi.org/10.1016/j.csite.2023.103462
[5] Jalili, Payam, Hossein Narimisa, Bahram Jalili, and D. D. Ganji. "Micro-polar nanofluid in the presence of thermophoresis, hall currents, and Brownian motion in a rotating system." *Modern Physics Letters B* 37, no. 01 (2023): 2250197. https://doi.org/10.1142/S0217984922501974
[6] Jasim, Abeer Majeed, and Abdul-Sattar J. A. Al-Saif. "New analytical solution formula for heat transfer of unsteady two-dimensional squeezing flow of a casson fluid between parallel circular plates." *Journal of Advanced Research in Fluid Mechanics and Thermal Sciences* 64, no. 2 (2019): 219-243.
[7] Jalili, Payam, Ali Ahmadi Azar, Bahram Jalili, and Davood Domiri Ganji. "Study of nonlinear radiative heat transfer with magnetic field for non-Newtonian Casson fluid flow in a porous medium." *Results in Physics* 48 (2023): 106371. https://doi.org/10.1016/j.rinp.2023.106371
[8] Sarada, Konduru, Ramanahalli J. Punith Gowda, Ioannis E. Sarris, Rangaswamy Naveen Kumar, and Ballajja C. Prasannakumara. "Effect of magnetohydrodynamics on heat transfer behaviour of a non-Newtonian fluid flow over a stretching sheet under local thermal non-equilibrium condition." *Fluids* 6, no. 8 (2021): 264. https://doi.org/10.3390/fluids6080264

[9] Jalili, Payam, S. M. Sharif Mousavi, Bahram Jalili, Pooya Pasha, and Davood Domiri Ganji. "Thermal evaluation of MHD Jeffrey fluid flow in the presence of a heat source and chemical reaction." *International Journal of Modern Physics B* (2023): 2450113. https://doi.org/10.1142/S0217979224501133

[10] Alhadhrami, A., C. S. Vishalakshi, B. M. Prasanna, B. R. Sreenivasa, Hassan AH Alzahrani, R. J. Punith Gowda, and R. Naveen Kumar. "Numerical simulation of local thermal non-equilibrium effects on the flow and heat transfer of non-Newtonian Casson fluid in a porous media." *Case Studies in Thermal Engineering* 28 (2021): 101483. https://doi.org/10.1016/j.csite.2021.101483

[11] Li, Yun-Xiang, M. Ijaz Khan, RJ Punith Gowda, Arfan Ali, Shahid Farooq, Yu-Ming Chu, and Sami Ullah Khan. "Dynamics of aluminum oxide and copper hybrid nanofluid in nonlinear mixed Marangoni convective flow with entropy generation: Applications to renewable energy." *Chinese Journal of Physics* 73 (2021): 275-287. https://doi.org/10.1016/j.cjph.2021.06.004

[12] Gowda, R. J. Punith, A. Rauf, R. Naveen Kumar, B. C. Prasannakumara, and S. A. Shehzad. "Slip flow of Casson-Maxwell nanofluid confined through stretchable disks." *Indian Journal of Physics* 96, no. 7 (2022): 2041-2049. https://doi.org/10.1007/s12648-021-02153-7

[13] Jalili, Bahram, Amirhossein Rezaeian, Payam Jalili, Davood Domeri Ganji, and Yasir Khan. "Squeezing flow of Casson fluid between two circular plates under the impact of solar radiation." *ZAMM-Journal of Applied Mathematics and Mechanics/Zeitschrift für Angewandte Mathematik und Mechanik* 103, no. 9 (2023): e202200455. https://doi.org/10.1002/zamm.202200455

[14] Gowda, R. J. Punith, R. Naveen Kumar, Umair Khan, B. C. Prasannakumara, Aurang Zaib, Anuar Ishak, and Ahmed M. Galal. "Dynamics of nanoparticle diameter and interfacial layer on flow of non-Newtonian (Jeffrey) nanofluid over a convective curved stretching sheet." *International Journal of Modern Physics B* 36, no. 31 (2022): 2250224. https://doi.org/10.1142/S0217979222502241

[15] Kumar, Rangaswamy Naveen, J. Suresh Goud, Pudhari Srilatha, Pattasale T. Manjunatha, S. Prasanna Rani, Raman Kumar, and S. Suresha. "Cattaneo-Christov heat flux model for nanofluid flow over a curved stretching sheet: An application of Stefan blowing." *Heat Transfer* 51, no. 6 (2022): 4977-4991. https://doi.org/10.1002/htj.22532

[16] Kumar, R. Naveen, RJ Punith Gowda, Mohammad Mahtab Alam, Irfan Ahmad, Y. M. Mahrous, M. R. Gorji, and B. C. Prasannakumara. "Inspection of convective heat transfer and KKL correlation for simulation of nanofluid flow over a curved stretching sheet." *International Communications in Heat and Mass Transfer* 126 (2021): 105445. https://doi.org/10.1016/j.icheatmasstransfer.2021.105445

[17] Zhao, Tie-Hong, M. Ijaz Khan, Sumaira Qayyum, R. Naveen Kumar, Yu-Ming Chu, and B. C. Prasannakumara. "Comparative study of ferromagnetic hybrid (manganese zinc ferrite, nickle zinc ferrite) nanofluids with velocity slip and convective conditions." *Physica Scripta* 96, no. 7 (2021): 075203. https://doi.org/10.1088/1402-4896/abf26b

[18] Abdulridah, Saja Isam, and Abeer Majeed Jasim. "New Analytical Study of Heat Transfer Analysis of Jeffery-Hamel Nanofluid Flow Problem with Porous Medium." *Journal of Advanced Research in Fluid Mechanics and Thermal Sciences* 103, no. 1 (2023): 105-132. https://doi.org/10.37934/arfmts.103.1.105132

[19] Jasim, Abeer Majeed. "Exploration of No-Slip and Slip of Unsteady Squeezing Flow Fluid Through a Derivatives Series Algorithm." *Journal of Advanced Research in Fluid Mechanics and Thermal Sciences* 100, no. 1 (2022): 11-29. https://doi.org/10.37934/arfmts.100.1.1129

[20] Khan, Ansab Azam, Khairy Zaimi, Suliadi Firdaus Sufahani, and Mohammad Ferdows. "MHD flow and heat transfer of double stratified micropolar fluid over a vertical permeable shrinking/stretching sheet with chemical reaction and heat source." *Journal of Advanced Research in Applied Sciences and Engineering Technology* 21, no. 1 (2020): 1-14. https://doi.org/10.37934/araset.21.1.114

[21] Kumar, R. S. Varun, B. Saleh, G. Sowmya, Asif Afzal, B. C. Prasannakumara, and R. J. Punith Gowda. "Exploration of transient heat transfer through a moving plate with exponentially temperature-dependent thermal properties." *Waves in Random and Complex Media* (2022): 1-19. https://doi.org/10.1080/17455030.2022.2056256

[22] Jalili, Bahram, Amirhossein Rezaeian, Payam Jalili, Fathollah Ommi, and Davood Domiri Ganji. "Numerical modeling of magnetic field impact on the thermal behavior of a microchannel heat sink." *Case Studies in Thermal Engineering* 45 (2023): 102944. https://doi.org/10.1016/j.csite.2023.102944

[23] Zhou, J. K. Differential Transformation and Its Application for Electrical Circuits. Huazhong University Press, 1986.

[24] Hatami, M., J. Hatami, M. Jafaryar, and G. Domairry. "Erratum to: Differential transformation method for Newtonian and Non-Newtonian fluids flow analysis: comparison with HPM and numerical solution." *Journal of the Brazilian Society of Mechanical Sciences and Engineering* 38 (2016): 1831-1831. https://doi.org/10.1007/s40430-016-0577-8

[25] Sobamowo, M. G. "Singular perturbation and differential transform methods to two-dimensional flow of nanofluid in a porous channel with expanding/contracting walls subjected to a uniform transverse magnetic field." *Thermal Science and Engineering Progress* 4 (2017): 71-84. https://doi.org/10.1016/j.tsep.2017.09.001

[26] Sowmya, Ganeshappa, Ioannis E. Sarris, Chandra Sen Vishalakshi, Ravikumar Shashikala Varun Kumar, and Ballajja Chandrappa Prasannakumara. "Analysis of transient thermal distribution in a convective-radiative moving rod using two-dimensional differential transform method with multivariate Pade approximant." *Symmetry* 13, no. 10 (2021): 1793. https://doi.org/10.3390/sym13101793

[27] Sowmya, G., R. S. Varun Kumar, M. D. Alsulami, and B. C. Prasannakumara. "Thermal stress and temperature distribution of an annular fin with variable temperature-dependent thermal properties and magnetic field using DTM-Pade approximant." *Waves in Random and Complex Media* (2022): 1-29. https://doi.org/10.1080/17455030.2022.2039421

[28] Kumar, Ravikumar Shashikala Varun, Rangaswamy Naveen Kumar, Ganeshappa Sowmya, Ballajja Chandrappa Prasannakumara, and Ioannis E. Sarris. "Exploration of temperature distribution through a longitudinal rectangular fin with linear and exponential temperature-dependent thermal conductivity using DTM-Pade approximant." *Symmetry* 14, no. 4 (2022): 690. https://doi.org/10.3390/sym14040690

[29] Mirzaaghaian, A., and D. D. Ganji. "Application of differential transformation method in micropolar fluid flow and heat transfer through permeable walls." *Alexandria Engineering Journal* 55, no. 3 (2016): 2183-2191. https://doi.org/10.1016/j.aej.2016.06.011

[30] Abdelghany, S. M., K. M. Ewis, A. A. Mahmoud, and Mohamed M. Nassar. "Vibration of a circular beam with variable cross sections using differential transformation method." *Beni-Suef University Journal of Basic and Applied Sciences* 4, no. 3 (2015): 185-191. https://doi.org/10.1016/j.bjbas.2015.05.006

[31] Hatami, M., and D. Jing. "Differential Transformation Method for Newtonian and non-Newtonian nanofluids flow analysis: Compared to numerical solution." *Alexandria Engineering Journal* 55, no. 2 (2016): 731-739. https://doi.org/10.1016/j.aej.2016.01.003

[32] Ganji, Hamed Faghanpour, Mohsen Jouya, Seyed Abbas Mirhosseini-Amiri, and Davod Domiri Ganji. "Traveling wave solution by differential transformation method and reduced differential transformation method." *Alexandria Engineering Journal* 55, no. 3 (2016): 2985-2994. https://doi.org/10.1016/j.aej.2016.04.012

[33] Bozyigit, Baran, Yusuf Yesilce, and Seval Catal. "Free vibrations of axial-loaded beams resting on viscoelastic foundation using Adomian decomposition method and differential transformation." *Engineering Science and Technology, An International Journal* 21, no. 6 (2018): 1181-1193. https://doi.org/10.1016/j.jestch.2018.09.008

[34] Tripathi, Dharmendra, Osman Anwar Bég, Praveen Kumar Gupta, Ganjam Radhakrishnamacharya, and Jagannath Mazumdar. "DTM simulation of peristaltic viscoelastic biofluid flow in asymmetric porous media: a digestive transport model." *Journal of Bionic Engineering* 12, no. 4 (2015): 643-655. https://doi.org/10.1016/S1672-6529(14)60154-2

[35] Stern, Ralph H., and Henning Rasmussen. "Left ventricular ejection: model solution by collocation, an approximate analytical method." *Computers in Biology and Medicine* 26, no. 3 (1996): 255-261. https://doi.org/10.1016/0010-4825(96)00007-8

[36] Nabati, Mohammad, Gholamreza Salehi, and Somaye Taherifar. "Numerical solution for a porous fin thermal performance problem by application of Sinc collocation method." *Mathematical Methods in the Applied Sciences* 46, no. 10 (2023): 11373-11391. https://doi.org/10.1002/mma.7740

[37] Vaferi, B., V. Salimi, D. Dehghan Baniani, A. Jahanmiri, and S. Khedri. "Prediction of transient pressure response in the petroleum reservoirs using orthogonal collocation." *Journal of Petroleum Science and Engineering* 98 (2012): 156-163. https://doi.org/10.1016/j.petrol.2012.04.023

[38] Biswal, Uddhaba, Snehashish Chakraverty, Bata Krushna Ojha, and Ahmed Kadhim Hussein. "Numerical simulation of magnetohydrodynamics nanofluid flow in a semi-porous channel with a new approach in the least square method." *International Communications in Heat and Mass Transfer* 121 (2021): 105085. https://doi.org/10.1016/j.icheatmasstransfer.2020.105085

[39] Shaoqin, Gao, and Duan Huoyuan. "Negative norm least-squares methods for the incompressible magnetohydrodynamic equations." *Acta Mathematica Scientia* 28, no. 3 (2008): 675-684. https://doi.org/10.1016/S0252-9602(08)60069-7

[40] Abbaszadeh, Mostafa, Mehdi Dehghan, Amirreza Khodadadian, Nima Noii, Clemens Heitzinger, and Thomas Wick. "A reduced-order variational multiscale interpolating element free Galerkin technique based on proper orthogonal decomposition for solving Navier-Stokes equations coupled with a heat transfer equation: Nonstationary incompressible Boussinesq equations." *Journal of Computational Physics* 426 (2021): 109875. https://doi.org/10.1016/j.jcp.2020.109875

[41] Hendi, Fatheah Ahmad, and Abeer Majed Albugami. "Numerical solution for Fredholm-Volterra integral equation of the second kind by using collocation and Galerkin methods." *Journal of King Saud University-Science* 22, no. 1 (2010): 37-40. https://doi.org/10.1016/j.jksus.2009.12.006

[42] Liberty, Ebiwareme, and Godwin Miracle. "The Comparison of Weighted Residual Methods of Solving Boundary Value Problems in Science and Engineering." *African Scholars Journal of pure and Applied Science* 18, no. 9 (2020): 19-32.
[43] Zhou, J. X., M. E. Li, Z. Q. Zhang, W. Zou, and L. Zhang. "A subdomain collocation method based on Voronoi domain partition and reproducing kernel approximation." *Computer Methods in Applied Mechanics and Engineering* 196, no. 13-16 (2007): 1958-1967. https://doi.org/10.1016/j.cma.2006.10.011
[44] Meher, Ramakanta, and Nirav D. Patel. "Analytical Investigation of MHD Jeffery-Hamel flow problem with heat transfer by differential transform method." *SN Applied Sciences* 1 (2019): 1-12. https://doi.org/10.1007/s42452-019-0632-z